Monthly Notices
of the
ROYAL ASTRONOMICAL SOCIETY

MNRAS **441,** 3209–3225 (2014) doi:10.1093/mnras/stu656

Radiolysis of amino acids by heavy and energetic cosmic ray analogues in simulated space environments: α-glycine zwitterion form

Williamary Portugal,[1] Sergio Pilling,[1]⋆ Philippe Boduch,[2] Hermann Rothard[2] and Diana P. P. Andrade[1,2]

[1] *Universidade do Vale do Paraíba (UNIVAP), São José dos Campos, SP, 12244-000, Brazil*
[2] *Centre de Recherche sur les Ions, les Matériaux et la Photonique CIMAP (GANIL/CEA/CNRS/ENSICAEN/Université de Caen Basse-Normandie), F-14070 Caen Cedex 05, France*

Accepted 2014 April 2. Received 2014 April 1; in original form 2013 November 7

ABSTRACT

In this work, we studied the stability of the glycine molecule in the crystalline zwitterion form, known as α-glycine ($^{+}NH_3CH_2COO^{-}$), under the action of heavy cosmic ray analogues. The experiments were conducted in a high vacuum chamber at the heavy-ion accelerator Grand Accélérateur National d'Ions Lourds (GANIL), in Caen, France. The samples were bombarded at two temperatures (14 and 300 K) by $^{58}Ni^{11+}$ ions of 46 MeV, up to a final fluence of 10^{13} ion cm^{-2}. The chemical evolution of the sample was evaluated in situ using a Fourier Transform Infrared Spectrometer (FTIR). The bombardment at 14 K produced several daughter species, such as OCN^{-}, CO, CO_2 and CN^{-}. The results also suggest the appearance of peptide bonds during irradiation, but this must be confirmed by further experiments. The half-life of glycine in the interstellar medium was estimated to be 7.8×10^3 yr (300 K) and 2.8×10^3 yr (14 K). In the Solar system, the values were 8.4×10^2 yr (300 K) and 3.6×10^3 yr (14 K). It is believed that glycine could be present in space environments that suffered aqueous changes, such as the interiors of comets, meteorites and planetesimals. This molecule is present in the proteins of all living beings. Therefore, studying its stability in these environments will provide further understanding of the role of this species in prebiotic chemistry on Earth.

Key words: astrobiology – astrochemistry – molecular data – methods: laboratory – cosmic rays – ISM: molecules.

1 INTRODUCTION

The interstellar medium (ISM), a vast space between stars, is a rich reservoir of gas and dust as well as organic compounds (e.g. Ehrenfreund & Charnley 2000). Denser regions of the ISM, called molecular clouds, are characterized by very low temperatures of the order of 10–30 K with densities around 10^4–10^8 particle cm^{-3}. Due to the low temperature, molecules from the gas phase are adsorbed on the surface of dust grains (aggregates of non-volatile species such as carbonaceous species, oxides and silicates), producing a water-rich ice mantle. In addition to amorphous water, interstellar ices consist of a variety of simple molecules such as CO_2, CO, CH_3OH and NH_3 (e.g. Boogert & Ehrenfreund 2004).

Laboratory studies have shown that the photolysis and radiolysis of space ice analogues can produce complex organic compounds and prebiotic molecules such as amino acids and nucleobases (e.g. Bernstein et al. 2002; Muñoz et al. 2002; Kobayashi et al. 2008; Pilling et al. 2009). The presence of these prebiotic compounds was also observed in laboratory investigations of meteorite samples, where more of the 70 amino acids were identified, as in the case of the Murchison meteorite (Cronin & Pizzarello 1983; Cronin, Pizzarello & Cruikshank 1988; Glavin & Dworkin 2009; Glavin et al. 2011).

Glycine (NH_2CH_2COOH), the simplest amino acid present in several proteins and enzymes in all forms of life on Earth, is predicted to exist in space (e.g. Kuan et al. 2003). Although this species has not yet been observed in the ISM, it was detected, together with some of its precursors, by chromatographic analysis and the carbon-isotope technique, in the samples collected from the 81P/Wild 2 comet and delivered to Earth by the NASA *Stardust* spacecraft (Elsila, Glavin & Dworkin 2009). This study reinforces the ideas of other authors (e.g. Chyba et al. 1990; Cronin, Pizzarello & Cruikshank 1988) that great amounts of organic materials could have been brought to Earth by comet and asteroid impacts. Research about this species helps our understanding of prebiotic chemistry, which could have been responsible for the emergence of life on the early Earth. Glycine in aqueous form is mainly zwitterionic glycine ($^{+}NH_3CH_2COO^{-}$: Pilling et al. 2013). However, in the condensed phase it is crystallized in different structures. According to Liu

⋆ E-mail: sergiopilling@pq.cnpq.br

et al. (2008), it can be found in three crystalline forms (α, β and γ-glycine), which are different from each other due to the angle between the C–N bond and the vibration mode around the C–C bond.

According to those authors, these three glycine forms are the consequence of the arrangement of the molecule on crystal structure and several kinds of interactions: (a) Van der Waals, (b) electrostatic and (c) hydrogen atom bond. The hydrogen bonds play an essential role in the organization of the crystallized glycine structure. According to Pilling et al. (2013), in space the glycine molecule can be formed by gas-phase reactions or on an ice surface by induced reactions. Radio observations have suggested that the abundance of glycine in space (gas phase) must be very low. However, if we consider that a small amount of glycine is present in the ISM and if it is continuously being produced from the gas phase and deposited on to grains or produced directly on grain surfaces (e.g. Woon 2002; Zhu & Ho 2004; Pilling et al. 2011a), its abundance on grains will increase with time during the evolution of an interstellar or protostellar cloud. Furthermore, the glycine desorbs only above ~400 K in high vacuum conditions (e.g. Pilling et al. 2013). Then, if such grains were exposed at temperatures around 200 K, all volatile compounds including water will be desorbed and the amount of glycine will increase with time, leading to the production of localized crystalline structures, such as β-glycine or α-glycine. These crystalline forms may exist in space, depending on the hydration degree, as discussed by Pilling et al. (2013). For example, due to radioactivity inside comets, a fraction of water may exist in the liquid phase, allowing the presence of α-glycine. The β-glycine form can be found in warm environments, H II regions and on dust of the diffuse intestellar medium (DISM), where water is absent. In astrophysical environments, at different temperatures, the glycine is exposed to several ionizing radiation fields (e.g. UV, X-rays and cosmic rays).

As discussed by Pilling et al. (2011a), the formation of amino acids from simple compounds such as CO, CO_2, CH_4, NH_3, H_2O and H_2 (and others) has been performed for at least 60 years in an attempt to simulate primitive Earth conditions (e.g. Miller 1953, 1955; Sanchez, Ferris & Orgel 1966; Ponnamperuma & Woeller 1967; Zhu & Ho 2004) or interstellar/protoplanetary grain mantles (e.g. Bernstein et al. 2002; Muñoz et al. 2002; Holtom et al. 2005; Elsila et al. 2007; Nuevo et al. 2008; Pilling et al. 2010a; de Marcellus et al. 2011). In most of those experiments, the gas mixtures or a film produced by the frozen gas mixtures are submitted to ionizing radiation sources (electrons, photons, fast ions and swift heavy ions), which trigger the physical chemistry reactions that allow complex molecules to be formed. The formation of glycine was also the subject of several theoretical studies involving different reactions set in the gas phase (e.g. Blagojevic, Petrie & Bohme 2003; Largo, Redondo & Barrientos 2003; Maeda & Ohno 2004; Bossa et al. 2009; Largo et al. 2010) and in or on interstellar grain analogues (e.g. Sorrell 2001; Woon 2002; Mendoza et al. 2004; Rimola & Ugliengo 2009).

In this work, we simulated in the laboratory the physical–chemical conditions found in space environments such as on the surface of grains inside denser regions of the ISM as well as grains in protostellar discs, comets and asteroids. The current experiments investigate the stability of glycine molecules in the condensed phase (crystalline zwitterionic form α-glycine) against heavy-ion cosmic ray analogues. The cross-sections obtained empirically here are compared with values obtained recently by Pilling et al. (2013) and Gerakines et al. (2012), employing light ions (~1 MeV protons) at different temperatures.

In Section 2, we present details of the experimental methodology. Results are presented in Section 3. These results are discussed in Section 4, including determination of the dissociation cross-section and the formation of daughter species (sample at 14 K). Astrophysical implications, involving half-life determination in different space environments with a radiation ionizing field, are discussed in Section 5. A summary containing our primary conclusions is in Section 6.

2 EXPERIMENTAL METHODOLOGY

The experiments were perfomed in a stainless steel chamber, under high vacuum conditions, coupled to the experimental beam line IRRadiation SUD (IRRSUD) of the heavy-ion accelerator Grand Accélérateur National d'Ions Lourds (GANIL), in Caen, France. The α-glycine crystal samples were prepared outside the vacuum chamber by drop casting of glycine aqueous solution (0.1 M) on CsI substrate. The sample was commercially bought from Sigma–Aldrich and had a purity of 99.9 per cent. The experiments were performed at two different temperatures: 14 and 300 K. The first sample was introduced inside the vacuum chamber and was bombarded at 300 K. The second sample was inserted into the chamber at 300 K and cooled to 14 K. After the bombardment at 14 K, the sample was heated slowly to room temperature. During this process, several infrared spectra were obtained from the sample to evaluate the changes due to the heating. During the experiment, the chamber pressure was around 2×10^{-8} mbar.

The samples were irradiated by $^{58}Ni^{11+}$ ions at an energy of 46 MeV. The flux was 2×10^9 ion cm^{-2} s^{-1}. The incoming charge of $q = 11^+$ is close to the mean charge of the ions inside the solid sample after several encounters with atoms in the target (Pilling et al. 2010a). The infrared spectra of glycine before and after different irradiation fluences (ion cm^{-2}) were obtained in situ with a Fourier Transform Infrared Spectrometer (FTIR; Thermo Nicolet – Magna 550), with wavenumbers ranging from 4000–650 cm^{-1} and with 1 cm^{-1} resolution. The spectrum of the clean CsI substrate was measured for background subtraction. Fig. 1 presents a schematic diagram of the experiment.

The molecular column density N was obtained from the relation between optical depth $\tau_\nu = \ln(I/I_0)$ and the band strength A (cm molecule^{-1}) of the respective vibration mode of a given species. Here, I_0 and I are the intensity of light before and after passing through a sample, respectively. Since the absorbance measured by FTIR is given by $Abs_\nu = \log(I_0/I)$, the column density of the samples according to Pilling et al. (2010a) is calculated by

$$N = \frac{1}{A}\int \tau_\nu \, d\upsilon = \frac{2.3}{A}\int Abs_\nu \, d\upsilon \qquad [\text{molecule cm}^{-2}], \qquad (1)$$

where $Abs_\nu = \ln(I/I_0)/\ln(10) = \tau\sqrt{2}.3$.

As discussed by Pilling et al. (2011), the thickness of the sample can be estimated by the expression

$$d = \frac{N_0}{6.02 \times 10^{23}}\frac{N}{\rho} \times 10^4 \qquad [\mu\text{m}], \qquad (2)$$

where N_0 is the initial column density in molecule cm^{-2}, M is the molar mass in g mol^{-1} and ρ is the glycine density in g cm^{-3}. In this work, we adopted the absorbance of the CN stretch vibration mode of glycine to determine the column density of the sample. The obtained value for the initial column density of α-glycine at 14 and 300 K was 1×10^{18} and 0.3×10^{18} cm^{-2}, respectively. Assuming 1.16 g cm^{-3} as the glycine average density in both samples, the sample thickness was estimated to be around 1–2 μm.

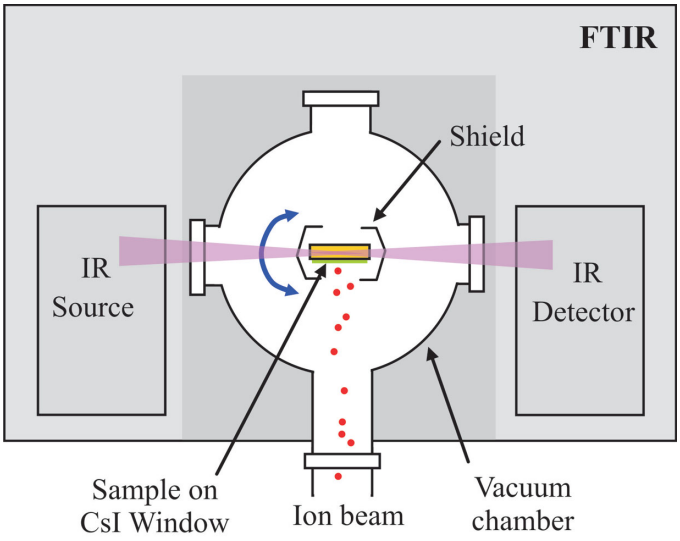

Figure 1. Schematic experimental set-up employed for bombardment of α-glycine crystal by heavy ions.

Due to the high velocity of incident $^{58}Ni^{11+}$ ions, energy deposition on the glycine sample is mainly by inelastic interactions with target electrons (electronic stopping power; Pilling et al. 2010a). Despite the ion flux employed in laboratory experiments being several orders of magnitude higher than the flux of similar ions in space and the thickness of laboratory ice also being higher, the energy delivered and the damage induced by similar ions in both scenarios have great similarity. Considering an energy of 46 MeV, we calculated, by means of the Stopping and Ranges of Ions in Matter (SRIM) software, the electronic and nuclear energy loss of projectiles in the glycine sample, which were 5270 keV μm^{-1} and 16.1 keV μm^{-1}, respectively. The maximum penetration depth of ions in the glycine sample was calculated to be 17.5 μm. In this case, the electronic stopping power is at least two orders of magnitude greater than the nuclear one. Then, the depth of penetration being one order of magnitude greater than the thickness of the sample, the ions cross the entire sample losing only about 10 per cent of their initial energy, ensuring an inelastic collision regime. These assumptions are in good agreement with the cosmic ray impact in submicron ices in interstellar or interplanetary regions, as discussed by Pilling et al. (2012).

In a similar experiment performed by Pilling et al. (2010a), the authors discussed the fact that each projectile induces significant changes in the sample only in a region of roughly 3 nm diameter. According to Pilling et al. (2012), considering a constant and homogeneous ion flux of 2×10^9 ion cm^{-2} s^{-1}, the average distance between two nearby impacts is roughly 300 nm (about 100 times higher than the length of the processed sample by a single projectile hit). From these values, the authors estimate that the probability of an ion hitting a given area of 3 nm diameter each second is about $P \sim 1.4 \times 10^{-4}$. Therefore, only after about 2 h of continuous bombardment does a second projectile hit in the same nanometric region. This is enough time to consider that each projectile always hits a thermalized region in the laboratory. According to Pilling et al. (2012), such a scenario is very similar to interstellar or interplanetary regions that have very low ion flux as well as ion fluence (even integrated over a large extended period of time). In this work, the maximum fluence (1×10^{13} ion cm^{-2}) employed in the bombardment of the sample was obtained after 1.5 h of direct exposure to cosmic ray analogues. Such a fluence corresponds to 10^6 yr of bombardment in the ISM, considering a flux of heavy ions ($12 \leq Z \leq 29$) with energy between 0.1 and 10 MeV in the ISM, estimated by Pilling et al. (2010a,b) as about 5×10^{-2} cm^{-2} s^{-1}.

3 RESULTS

The spectra obtained from non-irradiated and irradiated α-glycine samples at different fluences by $^{58}Ni^{11+}$ ions are shown in Fig. 2(a) and (b), respectively, for the samples at 14 and 300 K. Using these spectra, we can compare the effect of different fluences on the sample. In both figures, the non-irradiated crystalline sample is represented in the top spectrum. The arrow on the peak at 1034 cm^{-1} indicates the stretching vibrational mode of the C–N bond on the glycine molecule, employed to quantify the sample by means of equation (1). Beyond structural differences, crystals of α and β-glycine exhibit differences in their infrared spectra, for example band displacements (see details in Pilling et al. 2013). In the stretching vibration mode of C–N, α-glycine has a centre band at 1034 cm^{-1} and β-glycine at 1040 cm^{-1}.

The peak position and band strengths of some vibration modes of non-bombarded α-glycine crystal at 14 K are listed in Table 1 (taken from Holtom et al. 2005). In the glycine sample at 14 K, the bands at 2080, 2137, 2165, 2336 and 3280 cm^{-1} in Fig. 2(a) represent the daughter species CN^-, CO, OCN^-, CO_2 and H_2O, respectively, formed from irradiation of the sample (Pilling et al. 2010a; Gerakines et al. 1995). These species were produced from chemical processes triggered by heavy-ion-induced radiolysis. In the experiment at 300 K, new species could also be formed during the bombardment; however, due to the relatively high temperature of the sample, volatile species such as CO, CO_2 and H_2O may be desorbed and thus they were not found in the spectrum. The H_2O observed among daughter species may also have a contribution from the adsorption of residual gas in the back part of the CsI substrate, since the partial pressure of this compound inside a vacuum chamber is of the order of 1×10^{-8} mbar (∼1 monolayers adsorbed after each 100 seconds).

As described by Pilling et al. (2010a), the variation of the molecular abundance in the sample during the bombardment can be assigned to several processes: (i) molecular dissociation (quantified by the dissociation cross-section), (ii) molecular desorption (molecules

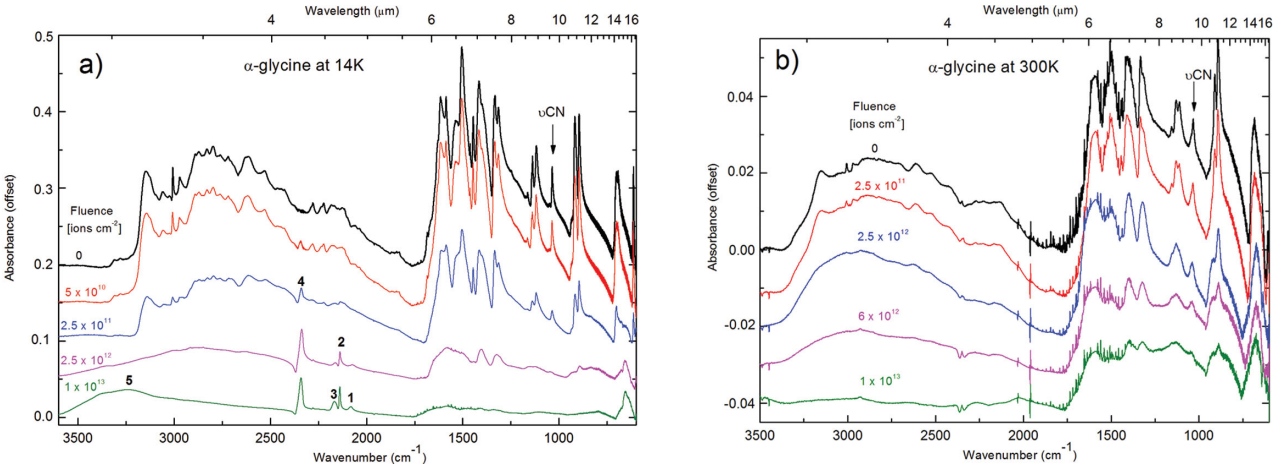

Figure 2. Infrared spectra of α-glycine ($^{+}NH_3CH_2COO^{-}$) before (top dark line) and after different irradiation fluences. The arrow on the peak at 1034 cm^{-1} indicates the location of the CN stretching mode employed to quantify the sample. The peaks of daughter species formed on the irradiated sample at 14 K are indicated by numbers: (1) CN^{-} (2080 cm^{-1}); (2) CO (2137 cm^{-1}); (3) OCN^{-} (2165 cm^{-1}); (4) CO_2 (2336 cm^{-1}); (5) H_2O (3280 cm^{-1}). Samples at (a) 14 K and (b) 300 K.

Table 1. Peak position (in cm^{-1} and μm) and band strength (also called *A* value) of some vibration modes of a non-bombarded α-glycine crystal at 14 K (taken from Holtom et al. 2005).

Position (cm^{-1})	Position (μm)	Assignment	Characterization	*A* value (cm molecule^{-1})
3076, 3040	3.2, 3.3	$\nu_{as}NH_3$	Asymmetric stretch	2.17×10^{-17}
1596	6.3	$\nu_{as}CO_2^-$	Asymmetric stretch	8.77×10^{-17}
1505	6.6	$\delta s\ NH_3$	Scissoring	4.39×10^{-17}
1413	7.1	$\nu_s CO_2^-$	Symmetric stretch	3.86×10^{-17}
1334	7.5	ωCH_2	Wagging	8.77×10^{-17}
1131	8.8	NH_3	Stretching	1.43×10^{-18}
1112	8.9	ρNH_3	Rocking	4.70×10^{-18}
1034	9.7	νCN	Stretching	1.38×10^{-18}

sublimated from the solid sample due to incident radiation) and (iii) formation of the new molecules (quantified by formation cross-section).

4 DISCUSSION

4.1 Dissociation cross-section of glycine under bombardment of NI ions

The dissociation (or destruction) cross-section (σ_d) of a given molecule under a given dissociation process is unique and should be reproducible at any laboratory. However, when we use the evolution of bands in the infrared spectra (molecular vibration modes) to determine such a value, we may have different approaches, as we will discuss further. In this work, we present another kind of cross-section called the specific bond rupture cross-section, which is conceptually different from the molecular dissociation cross-section and monitors the sensitivity of a given molecular bond to given dissociation processes such as ion bombardment.

The specific bond rupture cross-sections $\sigma_{(XY)}$ of a given molecule can be obtained from the expression

$$\ln\left(\frac{a}{a_0}\right) = -\sigma_{(XY)} \cdot F, \tag{3}$$

where a_0 and a are the integrated absorbance of a given vibration mode involving atoms *X* and *Y* observed in the infrared spectrum at the beginning of the experiments and at a given fluence, respectively. *F* is the fluence in units of ion cm^{-2}.

The degradation of the sample under action of $^{58}Ni^{11+}$ ions of 46 MeV is presented quantitatively in Fig. 3(a) and (b) for the experiments at 14 and 300 K, respectively. These figures show the peak area dependence as a function of the fluence (normalized to the initial peak area) for three different functional groups for the glycine molecule: CN, CH and NH. Since different bonds in the glycine molecule have different bond energies, they can also have different fragilities under irradiation (or ionizing fields), as illustrated by the different dissociation cross-sections of specific bonds. This difference in the dissociation cross-section for specific molecular bonds in a solid sample was also observed in similar experiments in the literature (e.g. Andrade et al. 2013; Pilling et al. 2013; Bergantini et al. 2014).

Below, we list three different methodologies that can be adopted for determination of the molecular dissociation cross-section (σ_d) of a given molecule directly from the evolution of bands in the infrared spectrum as a function of the fluence ionizing radiation.

(i) We can suppose that the molecular dissociation cross-section is ruled by the maximum value obtained for the specific bond rupture cross-section ($\sigma_{(XY)}$). This can be expressed as

$$\sigma_d = \max_{i=1,n} \sigma_{(XY)_i}. \tag{4}$$

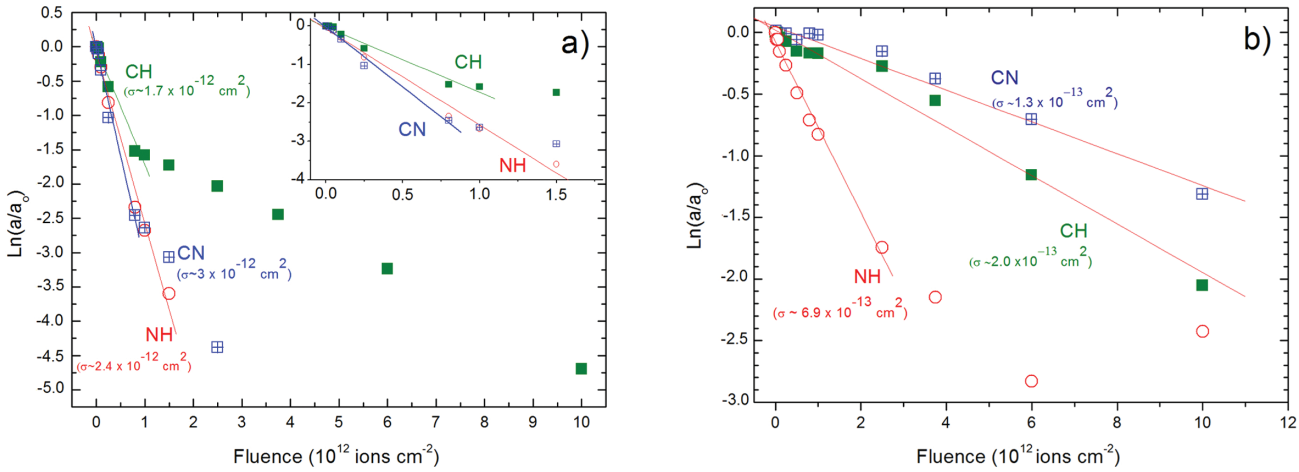

Figure 3. Evolution of the integrated absorbance of selected vibration modes (CN, CH and NH) of α-glycine crystal as a function of ion fluence. Samples are at (a) 14 K and (b) 300 K. Lines represent the best fit employing equation (3). The values of the cross-sections determined for specific bond ruptures are indicated in the figure.

Table 2. Cross-sections for specific bond ruptures $\sigma_{(CN)}$, $\sigma_{(C\text{-}H)}$ and $\sigma_{(N\text{-}H)}$ of the glycine molecule and the glycine dissociation cross-section (σ_d) due to the bombardment of 46-MeV Ni^{11+} at 14 and 300 K. For comparison purposes, the values obtained by Pilling et al. (2013) employing 1-MeV protons at 300 K are also given.

Cross-sections	Vibration mode	Value at 14 K (10^{-12} cm^2)	Value at 300 K (10^{-13} cm^2)	Ratio	Value obtained by Pilling et al. 2013. (10^{-14} cm^2)
$\sigma_{(CN)}$	C–N (νCN)	$\sim 3.0 \pm 0.3^a$	1.3 ± 0.1^a	23.1	2.5
$\sigma_{(CH)}$	C–H (ω CH_2)	1.7 ± 0.2^a	$\sim 2.0 \pm 0.2^a$	8.5	2.1
$\sigma_{(NH)}$	N–H ($\nu_{as}NH_3$)	2.4 ± 0.2^a	6.9 ± 0.7^a	3.5	3.1
σ_d	–	2.4 ± 0.4^b	3.4 ± 1.8^b	7.1^c	2.6^d

[a]The estimated errors are from the uncertainty in the band area determination (∼10 per cent).
[b]The molecular dissociation cross-section (σ_d) is given by the average value for the dissociation cross-section of specific bond rupture, as discussed in the text. The errors presented are the standard error of the values determined from the cross-section of specific bond ruptures.
[c]Obtained from the average values of the ratios listed above.
[d]The average value for σ_d calculated from Pilling et al. (2013).

However, in some cases this may introduce an additional error if we consider atoms that have very low bond energy (such as hydrogen atoms in the sp^3 orbital or CH bond), which can be easily interchanged with the surrounding molecules (matrix/solvent/substrate).

(ii) An alternative way is to suppose that the molecular dissociation cross-section is ruled by the value obtained for the cross-section of the rupture of a molecular bond within the molecular backbone, $\sigma_{(XY)\text{backbone}}$. This can be written as

$$\sigma_d \sigma_{(XY)\text{backbone}}. \quad (5)$$

An example of a molecular backbone bond in a glycine molecule is the CN bond (this methodology has been employed by Pilling et al. 2013). The value of the dissociation cross-section of glycine, considering the C–N bond rupture and the action of Ni ions, is about 23 times higher at low temperature than at room temperature. This may be due to the high density in the sample at 14 K, as pointed out previously by Pilling et al. (2013). Another explanation for this enhancement in the dissociation at low temperature is the possible reaction of newly formed species with each other and others already present in the sample. The C–N bond in the α-glycine molecule at 14 K was the most sensitive bond during the ion bombardment. Curiously, this bond is less sensitive in the sample at 300 K. For comparison, the values obtained by Pilling et al. (2013) employing 1 MeV protons on α-glycine crystals at 300 K are also given in Table 2. Comparing only the data at 300 K bombarded by different projectiles, we observe that the sensitivity of N–H bonds is much higher than that of other groups when heavy ions are employed. For proton bombardment, the molecular bonds are destroyed in a similar way in both cases.

(iii) However, the simple way to derive the molecular dissociation cross-section from measurements in the infrared is to consider the average value between the different specific bond rupture cross-sections (or in some cases the evolution of the entire area in the infrared band). In this work, we adopted this methodology, analysing the evolution of the rupture of three molecular bonds (CN, NH and CH) of the glycine molecule in the infrared spectrum during bombardment with 46-MeV Ni ions. Therefore, we write the glycine molecular dissociation cross-section as

$$\sigma_d = \sum_{i=1,n}^{n} \frac{\sigma_{(XY)_i}}{n} = \frac{\sigma_{(CN)} + \sigma_{(NH)} + \sigma_{(CH)}}{3}. \quad (6)$$

Considering this methodology, the values obtained at 14 and 300 K were $\sigma_d = 2.4 \times 10^{-12}$ and 3.4×10^{-13} cm^2, respectively. Such a methodology was also employed by Pilling et al. (2011c) in experiments on the processing of solid glycine by ionizing photons.

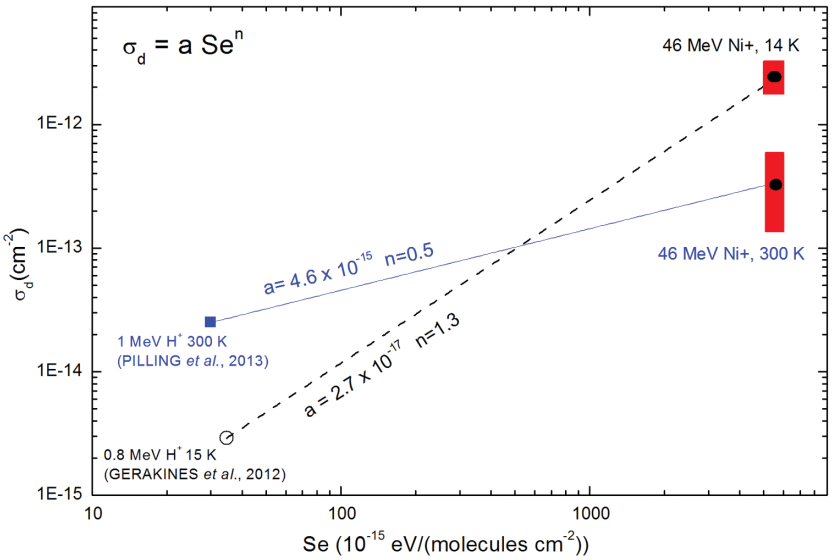

Figure 4. Dependence of glycine dissociation cross-section on the electronic stopping power at two temperatures (14 and 300 K). The circles represent the average values for the cross-section obtained from data of the $^{58}Ni^{11+}$ ion at 14 and 300 K in this work. The bars illustrate the range of values determined for the specific bond dissociation cross-sections in this work.

The error in the determination of the specific bond rupture cross-section lay in the uncertainty of the area determination in the infrared spectra, which was below 10 per cent. In this work, the estimated error for the glycine dissociation cross-section (σ_d) was adopted as equal to the standard error from the determined specific bond rupture cross-sections. This value was about 20 and 50 per cent for the experiments at 14 and 300 K, respectively. The values of the specific bond rupture cross-section and the glycine dissociation cross-section are listed in Table 2. The value of the dissociation cross-section considering the average value at low temperature is about seven times higher than that at room temperature. It is possible to see in Table 2 that, for any adopted vibration mode or considering average values, the glycine dissociation cross-sections are higher for the sample at 14 K.

4.2 Modelling the dissociation cross-section of glycine under the action of all energetic ions

In this work, the half-life of the glycine molecule was estimated considering interaction with several cosmic ray constituents. As discussed previously by Andrade et al. (2013), de Barros et al. (2014) and references therein, the dissociation cross-section of a frozen molecule under bombardment by heavy ions can be modelled by the power law

$$\sigma_d = aS_e^n, \quad (7)$$

where σ_d is the molecular dissociation cross-section in cm^2, S_e is the electronic stopping power and a and n are constants determined empirically. According to those authors, when ionic projectiles pass through the target material, they continually transfer their energies to the target and also induce an ionization process, resulting in a second generation of ions, radicals, electrons, photons and excited species. For ion beams with high velocities, the projectile energy and momentum are mainly transferred to the target by ion electron interaction (electronic stopping regime). The projectiles traverse each molecular layer, losing a small amount of their energy along the pathway, modifying its charge state and velocity. The electronic stopping power (S_e) was calculated using the SRIM code written by Ziegler, Biersack & Ziegler (2008).

Table 3. Best-fitting parameters from the equation of the dissociation cross-section as a function of electronic stopping power: $\sigma_d = aS_e$.

Temperature (K)	n	a
14	1.3	2.7×10^{-17}
300	0.5	4.6×10^{-15}

Fig. 4 shows the dependence of the glycine dissociation cross-section on the electronic stopping power at two temperatures (14 and 300 K). The black circles represent the average values for the cross-section obtained employing the $^{58}Ni^{11+}$ ion at 14 and 300 K (this work). The red bars illustrate the range of values determined for the specific bond dissociation cross-sections in this work. For H ions, we used S_e values of 0.8 and 1 MeV at 14 and 300 K, respectively, and cross-sections of 2.9×10^{-15} and 2.5×10^{-14} cm^2, according to data of Pilling et al. (2013) and Gerakines et al. (2012). The cross-section estimated for H ions (2.9×10^{-15} cm^2) from Gerakines et al. (2012) is for a glycine plus H_2O sample. In this work, we adopted the idea that the dissociation cross-section of glycine by Ni ions is the average value of three specific bond dissociation cross-sections, as listed in Table 2. Therefore the glycine dissociation cross-sections were $2.4 \pm 0.4 \times 10^{-12}$ and $3.4 \pm 1.8\ 10^{-13}$ cm^2 at 14 and 300 K, respectively. Lines show the best fits employing equation (7) for the two sets of data at two distinct temperatures. The values of the constants obtained from the models are indicated in the figure and also listed in Table 3.

The a and n values listed in Table 3 were used to calculate the destruction cross-sections (σ_d) of glycine molecules at 14 and 300 K under bombardment by several ions according to equation (7). The destruction cross-sections as a function of energy at 14 and 300 K, respectively, are presented in Fig. 5(a) and (b). This figure shows that, over a range of approximately 0.1–10 MeV (a.m.u.)$^{-1}$, cosmic rays promote higher destruction in the samples. In addition, in this

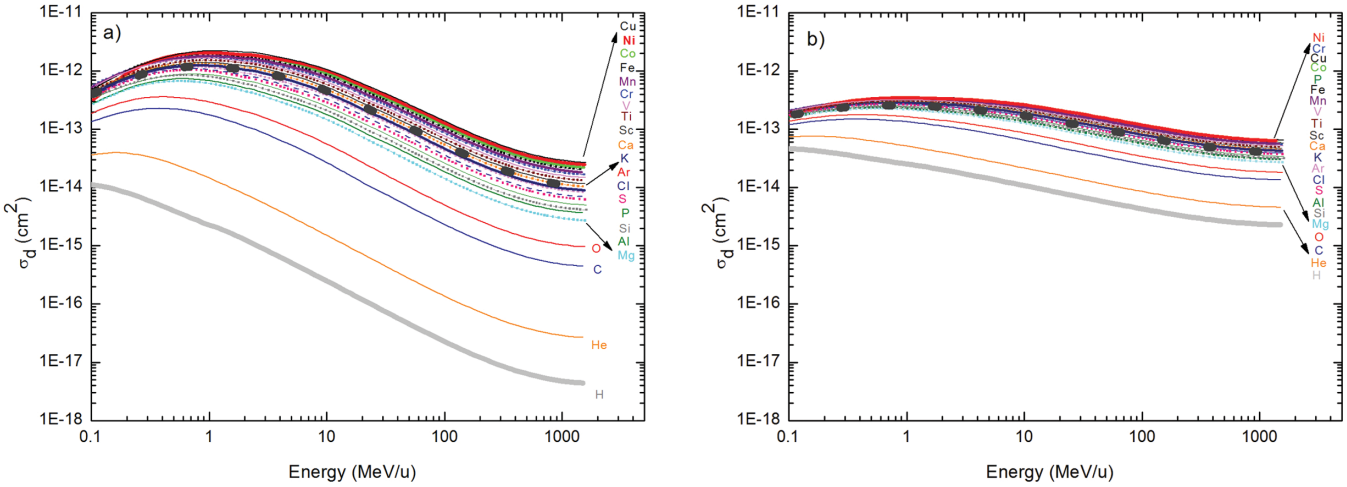

Figure 5. Destruction cross-section of glycine by cosmic rays as a function of energy, for experiments at (a) 14 K and (b) 300 K. See details in text. The large dashed line in both panels is the average value.

Table 4. Glycine dissociation cross-section considering different ions (main constituents of the cosmic ray inventory) at selected energies (0.1, 10 and 1000 MeV (a.m.u.)$^{-1}$) as well the average value. The estimated error at 14 K was around 20 per cent and that at 300 K was around 50 per cent. Such error values were determined mainly by the standard error of the glycine dissociation cross-section employing Ni ions, as illustrated in Table 2.

	0.1 MeV (a.m.u.)$^{-1}$		10 MeV (a.m.u.)$^{-1}$		1000 MeV (a.m.u.)$^{-1}$	
Ions	14 K	300 K	14 K	300 K	14 K	300 K
Al	2.8×10^{-13}	1.6×10^{-13}	1.7×10^{-13}	1.4×10^{-13}	4.0×10^{-15}	3.1×10^{-14}
Ar	3.6×10^{-13}	1.8×10^{-13}	3.8×10^{-13}	1.8×10^{-13}	9.1×10^{-15}	4.3×10^{-14}
Ca	4.6×10^{-13}	2.0×10^{-13}	4.8×10^{-13}	2.0×10^{-13}	1.1×10^{-14}	4.7×10^{-14}
Cl	3.8×10^{-13}	1.8×10^{-13}	3.3×10^{-13}	1.7×10^{-13}	7.5×10^{-15}	4.0×10^{-14}
Co	2.0×10^{-12}	3.4×10^{-13}	9.1×10^{-13}	2.5×10^{-13}	2.4×10^{-14}	6.3×10^{-14}
Cr	5.8×10^{-13}	2.1×10^{-13}	7.4×10^{-13}	2.3×10^{-13}	1.8×10^{-14}	'5.6×10^{-14}
Cu	5.0×10^{-13}	2.0×10^{-13}	1.0×10^{-12}	2.7×10^{-13}	3.0×10^{-14}	6.8×10^{-14}
Fe	5.2×10^{-13}	2.0×10^{-13}	8.6×10^{-13}	2.5×10^{-13}	2.2×10^{-14}	6.1×10^{-14}
K	4.2×10^{-13}	1.9×10^{-13}	4.1×10^{-13}	1.9×10^{-13}	9.7×10^{-15}	4.4×10^{-14}
Mg	2.7×10^{-13}	1.6×10^{-13}	1.4×10^{-13}	1.2×10^{-13}	3.0×10^{-15}	2.8×10^{-14}
Mn	5.3×10^{-13}	2.0×10^{-13}	7.8×10^{-13}	2.4×10^{-13}	2.0×10^{-14}	5.8×10^{-14}
Ni	3.2×10^{-13}	1.7×10^{-13}	9.8×10^{-13}	2.6×10^{-13}	2.7×10^{-14}	6.5×10^{-14}
P	3.5×10^{-13}	1.7×10^{-13}	2.4×10^{-13}	1.5×10^{-13}	5.4×10^{-15}	3.5×10^{-14}
S	3.6×10^{-13}	1.8×10^{-13}	2.9×10^{-13}	1.6×10^{-13}	6.8×10^{-15}	3.8×10^{-14}
Sc	4.4×10^{-13}	1.8×10^{-13}	5.3×10^{-13}	1.6×10^{-13}	1.3×10^{-14}	3.8×10^{-14}
Si	3.6×10^{-13}	1.8×10^{-13}	2.0×10^{-13}	1.5×10^{-13}	4.4×10^{-15}	3.3×10^{-14}
Ti	4.7×10^{-13}	2.0×10^{-13}	5.7×10^{-13}	2.1×10^{-13}	1.4×10^{-14}	5.1×10^{-14}
V	5.7×10^{-13}	2.1×10^{-13}	6.1×10^{-13}	2.2×10^{-13}	1.6×10^{-14}	5.4×10^{-14}
H	1.1×10^{-14}	4.7×10^{-14}	2.5×10^{-16}	1.1×10^{-14}	4.8×10^{-18}	2.4×10^{-15}
He	3.7×10^{-14}	7.4×10^{-14}	1.5×10^{-15}	2.2×10^{-14}	2.9×10^{-17}	4.7×10^{-15}
C	1.4×10^{-13}	1.2×10^{-13}	2.7×10^{-14}	6.5×10^{-14}	4.9×10^{-16}	1.4×10^{-14}
O	1.9×10^{-13}	1.2×10^{-13}	5.7×10^{-14}	6.5×10^{-14}	1.0×10^{-15}	1.4×10^{-14}
Average	4.1×10^{-13}	1.8×10^{-13}	4.5×10^{-13}	1.7×10^{-13}	1.1×10^{-14}	4.1×10^{-14}

energy range, the average of σ_d is higher at 14 K than at 300 K. For very high energies we observe the opposite behaviour. This can explain the low variation in half-life of the sample at 14 K, considering energy ranges of ~0.1–1.5 × 10^3 MeV (a.m.u.)$^{-1}$ and ~0.1–10 MeV. The initial energy studied for each ion is the energy at which S_e is at least ten times higher than S_n (nuclear stopping power), in the same energy range for all ions. This energy range is ~0.1–1.5 × 10^3 MeV (a.m.u.)$^{-1}$. The highest destruction cross-section rate for most ions (heavy ions) in the samples at both temperatures (14 and 300 K) occurs at about 1 MeV (a.m.u.)$^{-1}$. We also realize that the dissociation cross-sections of glycine irradiated by H and He, as a function of energy, are lower at 14 K than at 300 K. The glycine dissociation cross-section considering different ions (main constituents of the cosmic ray inventory) at selected energies (0.1, 10 and 1000 MeV (a.m.u.)$^{-1}$) as well the average value are presented in Table 4.

4.3 New species

For the sample bombarded at 14 K, it was possible to determine the formation cross-sections of the new species produced, such as OCN^-, CO_2, CO, CN^- and H_2O. For H_2O, this value must be

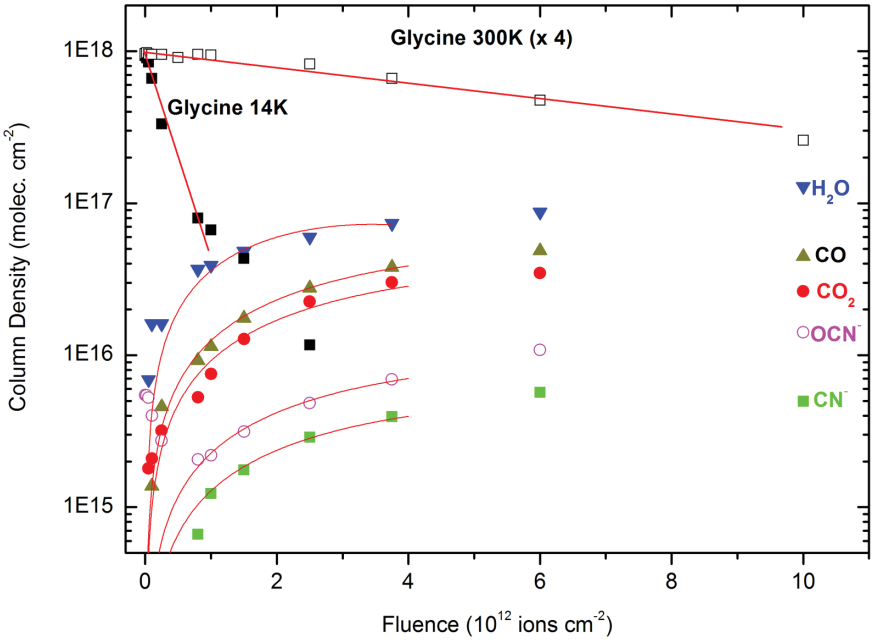

Figure 6. Chemical evolution of α-glycine bombarded by $^{58}Ni^{11}+$ ions at 14 K. For the sake of comparison, the evolution of the glycine column density in the experiment performed at 300 K is also presented. The red traces are the best fit obtained by equations (7) and (8).

employed with caution, due to the contribution of residual gas. As discussed by de Barros et al. (2011), the evolution of the column density of new species produced in the samples is best described by the equation

$$N_k = N_0 \sigma_{Fk} \left[F - \left(\frac{\sigma_d + \sigma_{dk}}{2} \right) F^2 \right], \quad (8)$$

where N_k is the column density of a given daughter species k in molecule cm^{-2}, N_0 is the initial column density of the parent species, F is the fluence in ion cm^{-2}, σ_{Fk} and σ_{dk} are the formation and dissociation cross-sections of daughter species in cm^2, respectively, and σ_d is the dissociation cross-section of the parent species.

Fig. 6 shows the chemical evolution of the sample at 14 K as a function of the fluence. We observe the decrease of glycine column density as a function of fluence, in contrast to the appearance of the new species produced: CN^-, CO, OCN^-, CO_2 and H_2O. For the sake of comparison, the evolution of the glycine column density in the experiment performed at 300 K is also presented. The column density evolution of glycine in both experiments was described by the simple relation

$$N = N_0 \exp(-\sigma_d F), \quad (9)$$

where N is the column density, N_0 the initial column density in molecule cm^{-2}, F the fluence in ion cm^{-2} and σ_d the dissociation cross-section in cm^2. The redcurves in Fig. 6 are the best fit obtained by employing equation (8) for the data of daughter species and equation (9) for the glycine data set.

From Fig. 6, we also observe that the abundance of water, as well as other daughter species, increases continually up to the end of the experiment. It is interesting to note that, at a fluence of approximately 1.5×10^{12} ion cm^{-2}, the amount of water produced is very similar to the amount of remaining glycine ($\sim 5 \times 10^{16}$ cm^2 = 5 per cent of glycine at the beginning of the experiment). For fluences higher than that, the sample composition does not show significant changes (excepting the large decrease of glycine as a function of the fluence). The decrease in glycine column density follows from equation (9). However, at low temperature this is only valid up to fluences around 1×10^{12} ion cm^{-2}. For higher fluences, we observe that the sample is slightly less destroyed as a function of fluence than at the beginning of the experiment. A similar behaviour was also observed by Pilling et al. (2013) in experiments bombarding α-glycine at 300 K with 1-MeV protons at fluences higher than 10^{14} ion cm^{-2}. Such behaviour may be explained by some compaction effect in the sample, changes in crystalline structure or newly produced glycine from the daughter species. This issue could be investigated by employing isotopic labelling of glycine (e.g. $NH_2CH_2^{13}COOH$) in future experiments.

The CN^-, CO_2 and CO molecules trapped in ice reached maximum production at about 6.0×10^{12} ion cm^{-2}. For fluences higher than that, their abundance decreased. As observed with the water molecule, the newly formed OCN^- increased as a function of the fluence. At a fluence around 1.0×10^{12} ion cm^{-2}, about 93 per cent of the glycine molecules (at 14 K) were dissociated by the action of cosmic rays and became daughter species (CN^-, CO, OCN^-, CO_2 and H_2O). The other 7 per cent may have suffered induced sputtering by the impact of heavy ions. The sputtering of frozen samples bombarded by heavy ions has been extensively described previously in the literature (Seperuelo et al. 2009; Pilling et al. 2010a,b).

The measurement of the column density of water in the experiments is a difficult task, because the IR bands of glycine also lie in the range of water bands. However, the following methodology was employed to estimate the column density of water: we integrated only the left side of the infrared absorbance profile of water (between wavenumbers 3628 cm^{-1} and 3300 cm^{-1}) and multiplied it by a factor of two. The left side of this band is virtually free from bands of other species present in the current experiment.

Table 5 shows the formation and dissociation cross-sections of some new species (CN^-, OCN^-, CO_2, CO and H_2O) identified during the bombardment of the α-glycine crystal at 14 K. The values were obtained by employing equation (8) for experimental data. The cross-section for H_2O should be used with caution, due to eventual contamination by the residual gas. The production of water from

Table 5. Formation cross-sections of the newly produced species from the bombardment of glycine by 46-MeV Ni^{11+} at 14 K. The estimated experimental error was below 10 per cent.

Daughter species	σ_{Fk} (10^{-14} cm^2)	σ_{dk} (10^{-13} cm^2)
CN^-	0.1	<0.1
OCN^-	0.2	<0.1
CO_2	1.0	<0.1
CO	1.3	<0.1

*The cross-section for H_2O should be used with caution, due to eventual contamination by the residual gas.

the bombardment of glycine species may also be related to the formation of peptide bonds, but other chemical pathways can also lead to water formation. Future experiments with isotopic labelling using glycine with ^{18}O will help to clarify this issue.

As discussed by Andrade et al. (2008) and Pilling et al. (2010a), the energy delivered by the incoming projectiles (about 46 MeV $\sim$ 7.3 $\times$ 10^{-12} J) induces several physical–chemical changes in the target. Basically, four main distinct physical–chemical regions in the target are produced, due to the radial energy gradient centred on the ion track.

(i) Region A (track region): a small cylinder-like shaped region ($d \sim 3$ Å) along the ion track, in which the energy delivered is so high that all the molecules of the target are completely atomized (for energies $E \gg 1$ keV).

(ii) Region B (ionization/dissociation region): a region ($d \sim 30$–100 Å) surrounding region A, in which the energy is not enough to atomize the target but induces bond ruptures (dissociation) and electron loss (ionization; for energies 1 keV $\gtrsim E \gtrsim$ 5 eV). The emission of secondary electrons inside this regions is also another source of energy input for chemical reactions. After ion bombardment, the molecules within this region can be converted to radicals that may react to produce new species such as CO, CO_2, OCN^- and amides. Moreover, the energy available there can be high enough to allow some reactions that have high values of activation barrier to occur, such as the formation of peptide bonds between two amino acids.

(iii) Region C (morphological changes region): a region far from the ion track ($d >$ 1000 Å) in which the energy available is not very high, inducing only morphological changes in the sample, such as changes in the crystalline structure and intermolecular bond ruptures (for energies $E \ll 5$ eV).

(iv) Region D: a plume-like shaped region outside the surface which contains ejected ionic and atomic species, radicals and molecular clusters sputtered from the sample. Some reactions in the gas phase may occur inside this region, depending of the number density and energy of the fragments. Details about the production of molecular clusters in this region can be obtained from Collado et al. (2004) and Andrade et al. (2008).

Fig. 7 shows a schematic diagram of these four different physical–chemical regions surrounding the ion track during the bombardment of the glycine sample. Selected reaction pathways for some daughter species, as well the suggested peptide bond formation that can occur in region B and a schematic plot of the energy delivered within the sample as a function of the distance of the ion track, are also shown. The peptide bond occurs through the link between the carboxyl group of one amino acid and the amine group of another amino acid, forming an amide group with the release of a water molecule. Such intermolecular bonds between amino acids provide the base for the production of longer molecular chains, including proteins.

Possible evidence of peptide bond formation was also suggested by Pilling et al. (2013) in similar experiments employing light-ion cosmic ray analogues (1 MeV protons) by the appearance of a peak around 1650 cm^{-1} in the IR spectra of the bombarded glycine

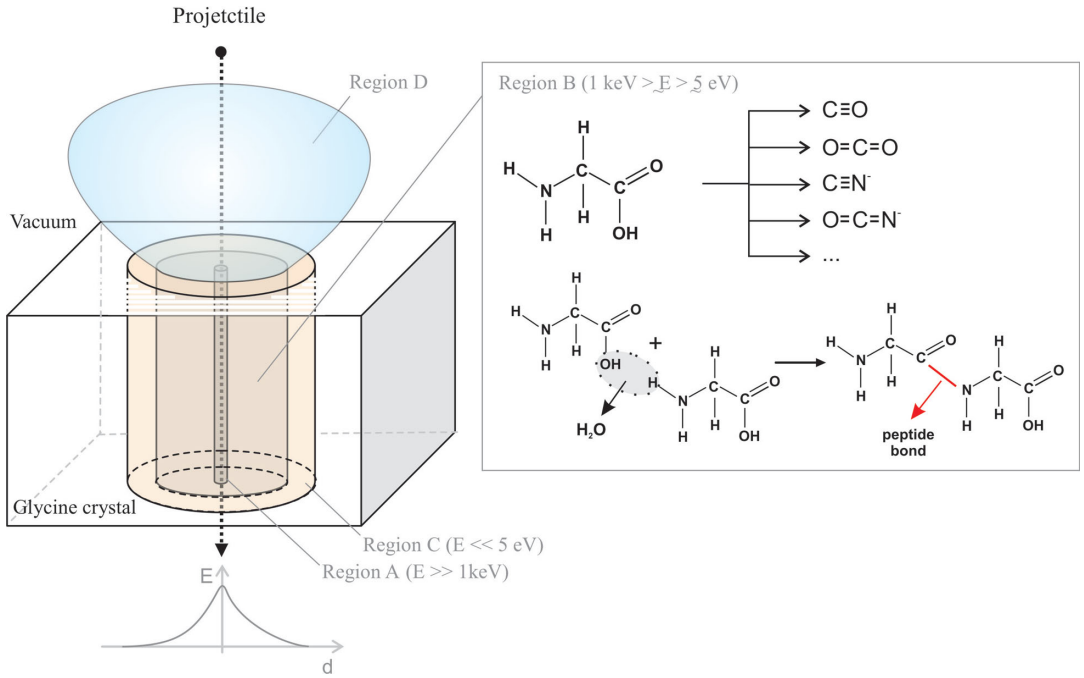

Figure 7. Schematic diagram of the three different physical–chemical regions surrounding the ion track during the bombardment of the glycine sample (named as regions A, B, C and D). Selected reaction pathways for some daughter species that can occur in region B and a schematic plot of the energy delivered within the sample as a function of the distance of the ion track are also shown. A tentative reaction for eventual production of the peptide bond is also illustrated. See details in the text.

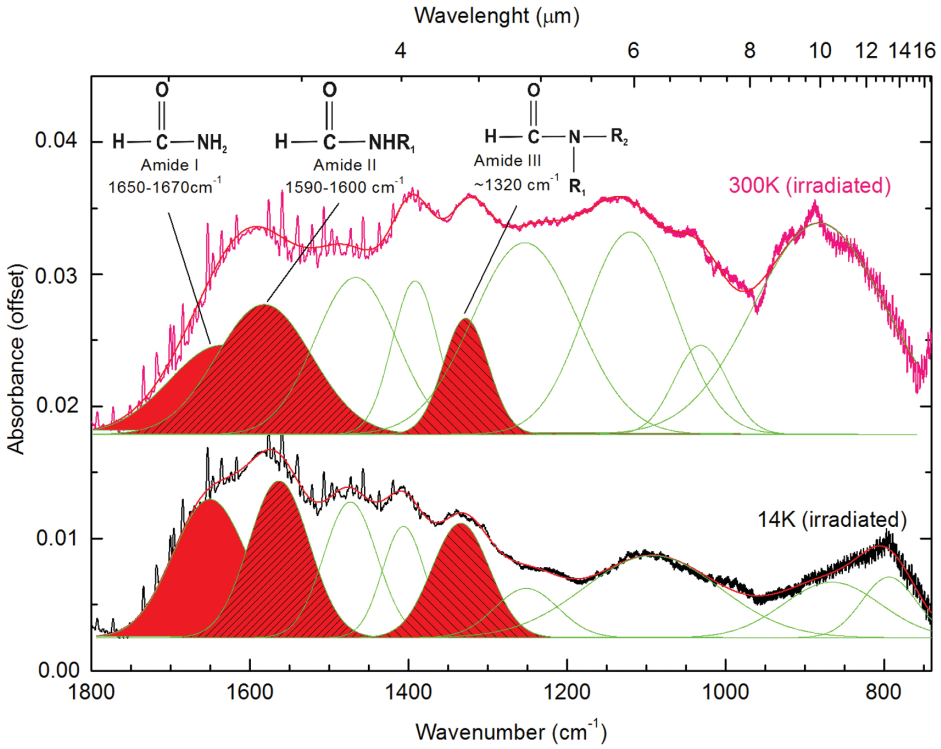

Figure 8. Expanded view of infrared spectra of the residues produced after the bombardment employing 1×10^{13} Ni ion cm^2. Filled curves present tentative assignments of amide bands obtained from a spectral deconvolution employing nine Gaussian profiles, in the range 1800–750 cm^{-1}.

samples, which was attributed to the amide bond. In addition, according to Kaiser et al. (2013), the formation of amino acid polymers, especially dipeptides, is of crucial relevance to the prebiotic processes that preceded the onset of life on Earth. Once delivered to the planet by meteorites and comets (Oró 1961), dipeptides could have acted as catalysts in the formation of sugars and enzymes (Weber & Pizzarello 2006). Kaiser et al. (2013), in an experiment simulating interstellar analogue ices at 10 K containing a mixture of different gases (e.g. carbon dioxide, ammonia and hydrocarbons) bombarded by energetic electrons, also found intense absorption profiles in the IR spectra, between wavenumbers ∼1600 and 1700 cm^{-1}, attributed to amide bonds. The chromatographic analysis of organic residues from such experiments at room temperature has shown nine different amino acids and at least two dipetides: Gly–Gly and Leu–Ala.

A comparison between the infrared spectra (from 1800–750 cm^{-1}) of the residues produced after a bombardment of 1×10^{13} Ni ion cm^2 of the two glycine samples is shown in Fig. 8. The two infrared profiles presented were adjusted by a sum of nine different Gaussians, representing different infrared profiles of molecular vibration modes. The Gaussian profiles centred around 1650–1670, 1590–1690 and ∼1320 cm^{-1} were tentatively assigned to the amide I, amide II and amide III bands, respectively, following the discussions presented by Kaiser et al. (2013) and Reis et al. (2006).

4.4 Heating of the sample

After bombardment by heavy ions, the sample at 14 K was slowly heated up to room temperature while in high vacuum conditions. During this process, several infrared spectra were taken to evaluate the chemical changes during heating. Examples of these spectra are presented in Fig. 9. This figure shows the evolution of the IR spectra from 3550–600 cm^{-1} of the α-glicina sample, bombarded at a fluence of 1×10^{13} ion cm^{-2} at 14 K, during heating to room temperature. The temperature of each spectrum is indicated. For sake of comparison, the upper spectrum shows data of the non-bombarded sample at 14 K. The band associated with CO (∼2137 cm^{-1}) is the first band to disasappear during the heating, indicating the fast evaporation of CO. This species was completely desorbed at 100 K. Some crystalline changes in the water profile at 3300 cm^{-1} are also observed in the spectrum obtained at 100 K. The spectrum at 180 K shows that molecules such as CO_2 (∼2336 cm^{-1}) and CN^- (2080 cm^{-1}) are also completely desorbed from the sample and water represents only a small fraction of the sample. During the sample heating, the OCN^- band, initially at 2165 cm^{-1} in the spectrum at 14 K, seems to shift to shorter wavenumber (longer wavelength). This behaviour was also observed by Pilling et al. (2010a) in H_2O:NH_3:CO (1:0.6:0.4) ice bombarded in similar conditions. The authors suggest that such a band observed at higher temperatures may be associated with a non-volatile aliphatic isocyanide R–N ≡ C (∼2150 cm^{-1}).

Fig. 10 presents the spectra of bombarded glycine at a fluence of 1×10^{13} ion cm^{-2} at 14 K (second lowermost curve) and 300 K (uppermost curve). For comparison purposes, the spectrum of bombarded glycine at 14 K following heating to 300 K (middle curve) and spectra of virgin glycine at 14 K (lowermost curve) and 300 K (second uppermost curve) are also shown.

As discussed previously, the CO (∼2137 cm^{-1}), CN^- (2080 cm^{-1}), CO_2 (∼2336 cm^{-1}) and H_2O (∼3280 cm^{-1}) formed at 14 K are not observed in the spectrum of processed glycine heated to 300 K (as can be seen in Fig. 9), suggesting that they were desorbed. The molecule OCN^- was not observed in the sample bombarded at 300 K; however, this species is present in small amounts in the spectrum of the bombarded sample heated to 300 K. This suggests

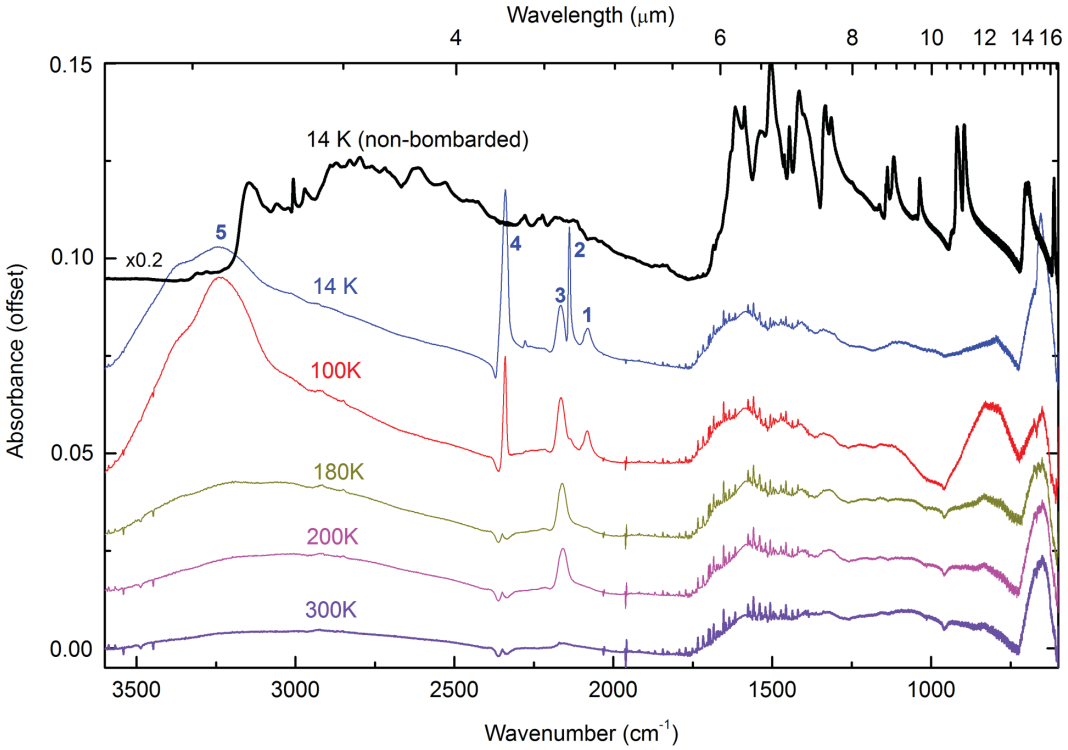

Figure 9. Infrared spectra of bombarded glycine at a fluence of 10^{13} ion cm^{-2} during heating from 14 to 300 K. For the sake of comparison, the upper spectrum shows the data of the non-bombarded sample at 14 K. The peaks of daughter species formed on the irradiated sample at 14 K are indicated by numbers: (1) CN^- (2080 cm^{-1}); (2) CO (2137 cm^{-1}); (3) OCN^- (2165 cm^{-1}); (4) CO_2 (2336 cm^{-1}); (5) H_2O (3280 cm^{-1}).

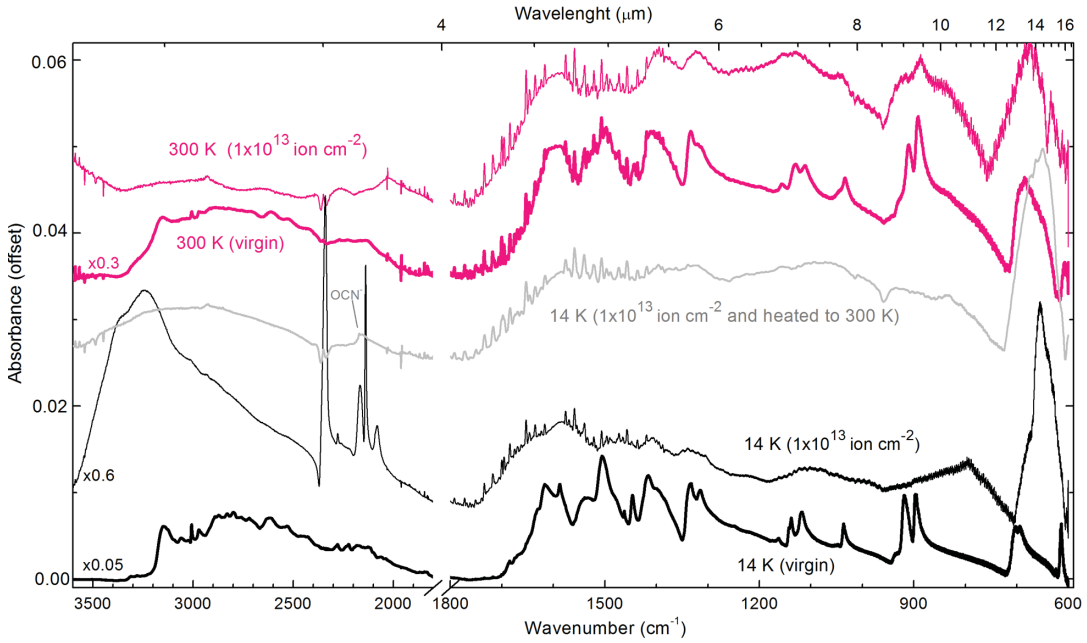

Figure 10. Spectra of bombarded glycine at a fluence of 1×10^{13} ion cm^{-2} at 14 K (bottom curve) and 300 K (upper curve). For comparison purposes, spectra of bombarded glycine at 14 K following heating to 300 K (middle curve) and of virgin samples at 14 and 300 K are also shown. See details in the text.

that a fraction of OCN^- (or other XCN^- species) may be trapped inside the crystalline structure of the bombarded sample at 14 K and is still there after sample heating to 300 K. Such a possible trapping scenario of newly produced species triggered by ion bombardment in ices was simulated theoretically by Anders & Urbassek (2012).

5 ASTROPHYSICAL IMPLICATIONS

The delivery of simple organic species found in the ISM, such as CH_4, H_2CO, CH_3OH, to the early Earth by comets and meteorites has been suggested as the most important source for the formation

of prebiotic organic compounds such as amino acids (e.g. Cronin, Pizzarello & Cruikshank 1988; Glavin & Dworkin 2009). There is also a long-standing hypothesis in the literature that molecular precursors important for the origin of life on Earth were first formed in space and subsequently delivered to Earth through impact events (Oró 1961; Chyba & Sagan 1992). Glycine, the simplest amino acid found in the proteins of all life forms on Earth, has not yet been found in the ISM. According to Holtom et al. (2005), an upper limit for the column density of this species in molecular clouds could be about 10^{12}–10^{14} molecule cm^{-2}, but the amount of interstellar glycine in the gas phase is still unknown. It is an open question whether glycine is abundant enough to become crystalline in space environments. Bernstein et al. (2002), by means of a laboratory demonstration, showed that glycine can be produced from ultraviolet photolysis of the analogues of icy interstellar grains. The stability of glycine in the presence of ionizing space agents has been studied by several research groups, for example involving UV (e.g. Ehrenfreund et al. 2001; Peeters et al. 2003; ten Kate et al. 2005; Guan et al. 2010; Ferreira-Rodrigues et al. 2011), X-rays (e.g. Pilling et al. 2011b), electron beams (Abdoul-Carime & Sanche 2004) and fast ions (Gerakines et al. 2012; Pilling et al. 2013). For this, space environments are simulated in the laboratory in order for the survival of molecules during the formation of the Solar system (SS) and the early Earth to be investigated.

The flux of Galactic cosmic ray ions in the ISM can be obtained by the equation

$$\phi_Z(E) = \frac{C_Z E^{0.3}}{(E+E_0)^3} \quad [\mathrm{cm^{-2}\,s^{-1}(MeV\,(a.m.u.)^{-1})^{-1}}] \qquad (10)$$

given by Webber & Yushak (1983), based on measurements of $_1$H, $_2$H, $_3$He and $_4$He made from balloons and *Voyager*. E_0 is a form parameter between 0 and 940 MeV. Changes in E_0 will change the spectra of low-energy cosmic rays substantially, but have almost no effect at the high-energy end. Smaller values of E_0 represent more low-energy cosmic ray particles (Shen et al. 2004). Webber & Yushak (1983) found that $E_0 = 300 \pm 100$ MeV can explain the measured ^{3}He/^{4}He ratio and their observed spectra very well. We assumed $E_0 = 400$ MeV, determined by Shen et al. (2004) as the best value for estimating the fluxes. In this equation, C_z is the normalization constant, which can be estimated for all ions as a function of the abundance of H in cosmic rays of 10^6 atoms and the normalization constant $C_1 = 9.42 \times 10^4$. Employing the ion abundances taken from Drury, Meyer & Ellison (1999), we calculated the normalization constant for other ions as $C_z = 9.42 \times 10^4$ ($n_z/10^6$). Here, n_z indicates the number density of a given atom of atomic number Z as a function of the number density of hydrogen atoms. For atoms for which data regarding the number density are unavailable (e.g. Cl, K, Sc, Ti, V, Cr and Mn), we used an average. The constant C_z of each ion as a function of the hydrogen abundance and the respective relative abundances in the ISM are presented in the Appendix (Table A1).

Inside the SS, the flux density of the solar wind plus solar energetic particles of cosmic rays can be estimated by the equation given by de Barros et al. (2011):

$$\phi_Z(E) = A_1 \exp(-\eta E) + \frac{A2}{(E)^2} \quad [\mathrm{cm^{-2}\,s^{-1}(MeV\,(a.m.u.)^{-1})^{-1}}], \qquad (11)$$

where A_1 and A_2 are parameters used to estimate the flux density of solar energetic particles in regions of low and high energy, respectively, according to the energy range given in de Barros et al. (2011). In this work, only the regions with the highest energies were studied, so the A_1 parameter was disregarded. A_2 was estimated for all ions by functions of atomic abundance. So we used the abundance and the A_2 value of H in the solar wind given by de Barros et al. (2011), being 3×10^8 atom and 46, respectively. With the abundance values of ions in the SS from Drury et al. (1999), we normalize these values as a function of the number density of hydrogen (3×10^8 atom) and estimate the A_2 of all other ions as $A_{2z} = 46\,(n_z/3 \times 10^8)$, where n_z indicates the number density of a given atom of atomic number Z as a function of the number density of hydrogen atoms in the SS. The A_2 values and the hydrogen relative abundance in the SS are also presented in the Appendix (Table A1). The variable E is the energy studied in the range $\sim$0.1–1.5 $\times$ 10^3 MeV (a.m.u.)$^{-1}$ and η is a parameter that is about 2400 for He, Fe and O (de Barros et al. 2011).

Once $\Phi_Z(E)$ and $\sigma_{\mathrm{d},z}(E)$ are known, the half-lives (τ) of the glycine molecule in the ISM and SS at 14 and 300 K due to cosmic ray irradiation could be evaluated using equation (12). The half-life of glycine, by Andrade et al. (2013), for the energy range $\sim$0.1–1.5 $\times$ 10^3 MeV (a.m.u.)$^{-1}$ in the ISM, was estimated to be 7.8×10^3 years (300 K) and 2.8×10^3 years (14 K). In the SS, the values were 8.4×10^2 yr (300 K) and 3.6×10^3 yr (14 K). We estimated other half-life values by the same methodology, changing the energy range and cosmic ray ion composition.

Fig. 11(a) and (b) shows the differential dissociation rate of glycine by cosmic rays in the ISM at 14 and 300 K, respectively. The differential dissociation rate is a parameter defined as the product between the fluxes of ions and their respective cross-sections as a function of energy ($\Phi(E) \times \sigma_{\mathrm{d}}(E)$). Fig. 12(a) and (b) shows the same parameter, but for the SS. According to these figures, the differential dissociation rate of glycine induced by cosmic rays ($\Phi(E) \times \sigma_{\mathrm{d}}(E)$) in the ISM predominates between approximately 0.1 and 10 MeV (a.m.u.)$^{-1}$; it is higher for the sample at 14 K that that at 300 K. As already discussed, this could be due to the high density in the sample at low temperature, enabling the dissociation of a higher number of molecules under the impact of cosmic rays. Furthermore, the dissociation of molecules by reactions between the species formed and others already present in the sample can occur. Fe (black line) is the element that predominates in glycine dissociation in the ISM. According to Fig. 12(a) and (b), H (grey line) and He (orangeline) are the ions that predominate in molecule dissociation in the SS. The values presented in Table 6 show this relation between cosmic ray composition and the energy ranges studied. The highest dissociation rate is found in the SS, because the fluxes of H and He integrated over energy in this environment are higher than in the ISM. Furthermore, the glycine dissociation cross-sections in relation to these ions are higher in the hottest environments (see Table 4). In addition, the work of Andrade et al. (2013) with formic acid at 15 K, irradiated by cosmic ray analogues, showed that protons and galactic He interact with deeper layers of ice. The SRIM calculations show that H and He ions have the highest perpendicular penetration depth during the bombardment. The S_e of other ions increases initially and then decreases. This can explain a higher molecule dissociation rate under the action of cosmic rays including the action of H and He ions, at both temperatures (14 and 300 K) and for the two energy ranges studied ($\sim$0.1–1.5 $\times$ 10^3 MeV (a.m.u.)$^{-1}$ and $\sim$0.1–10 MeV (a.m.u.)$^{-1}$). The glycine dissociation rate decreases when these ions are not taken into account, therefore increasing the half-life of the molecule during bombardment.

According to Andrade et al. (2013), by integrating the differential dissociation rate over energy ($\int \phi_z(E)\sigma_{\mathrm{d},z}(E)\,\mathrm{d}E$, it is possible to estimate the half-life of glycine in the ISM and SS, at two temperatures

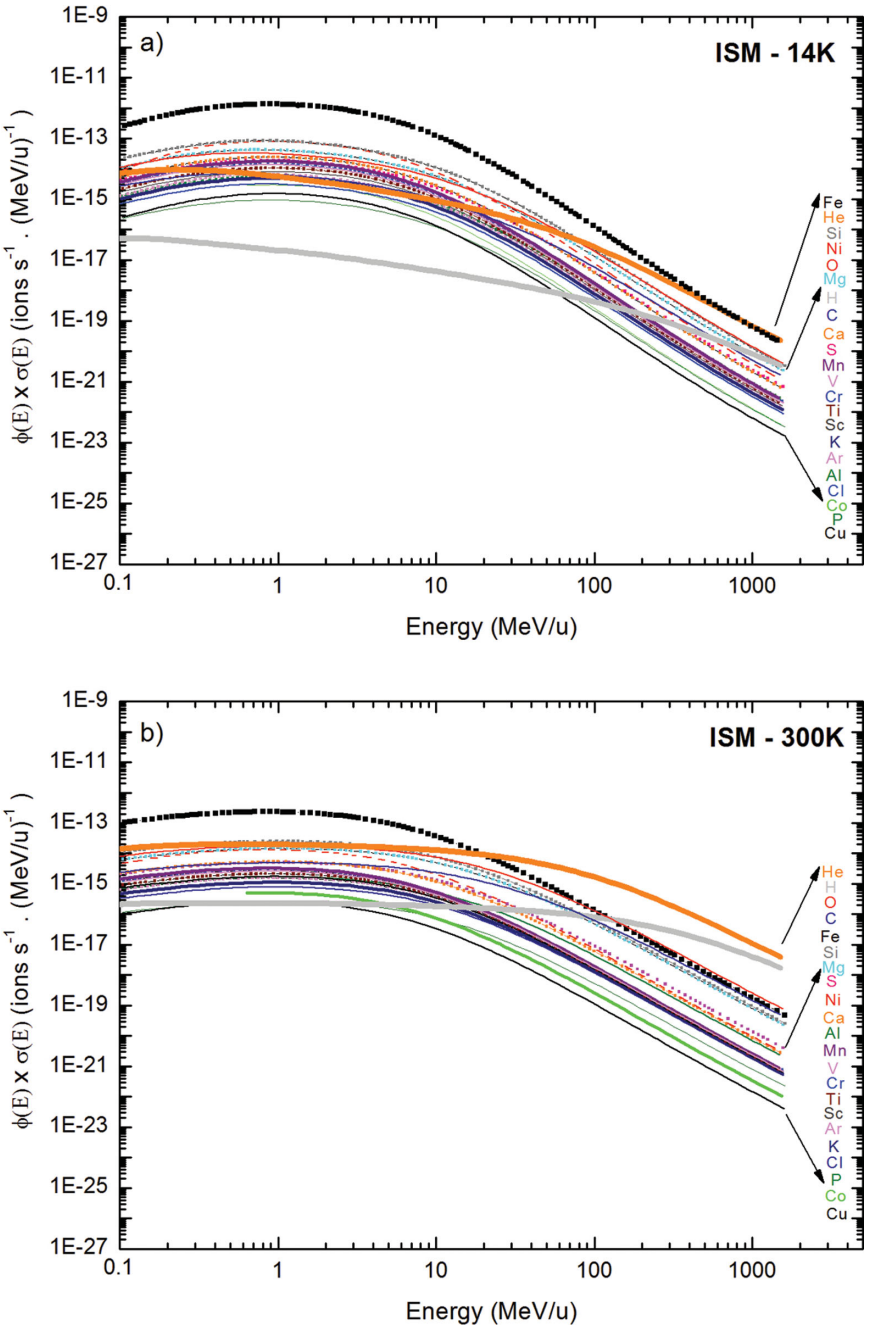

Figure 11. Differential dissociation rate of glycine by cosmic rays in the ISM as a function of energy, for experiments at (a) 14 K and (b) 300 K.

(14 and 300 K), by the equation

$$\tau = \frac{\ln(2)}{k} \quad [\mathrm{s}], \tag{12}$$

where k is the sum $\Sigma j \int \Phi_z(E)\sigma_{\mathrm{d},z}(E)\,\mathrm{d}E$, Φ_z is the estimated flux density of cosmic rays ($\Phi_{\mathrm{HCR}}(E)$) between E and $E + \mathrm{d}E$ in units of ion cm^{-2} s^{-1} (MeV (a.m.u.)$^{-1}$)$^{-1}$ and $\sigma_{\mathrm{d},z}$ is the destruction cross-section in cm^2, which is a function of the ion energy of a given ion with atomic number Z. The integration was performed over the whole energy range studied (∼0.01–1.5 × 10^3 MeV (a.m.u.)$^{-1}$) over the area below a given curve in Figs 11 and 12. The sum $\Sigma j \int \Phi_z(E)\sigma_{\mathrm{d},z}(E)\,\mathrm{d}E(k)$ was performed using the methodology suggested by Andrade et al. (2013) for all galactic cosmic ray ions studied, including H, He, C, O and the heavy ions ($12 \leq Z \leq 29$). In this work, we defined k' as the estimated value for the ionization rates, taking into account only those ions with energies in range 0.1–10 MeV. Table 6 presents these defined ionization rates k and k' for the glycine molecule in the ISM and SS at 14 and 300 K, exposed to cosmic rays in energy ranges ∼0.1–1.5 MeV (a.m.u.)$^{-1}$ and ∼0.1–10 MeV (a.m.u.)$^{-1}$. For comparison purposes, the ionization rates considering only heavy ions (named as k_{HCR} and k'_{HCR}) are also listed in this table.

To make comparison between the current data and previous works easier, we also calculated the half-life (τ*) of α-glycine crystals

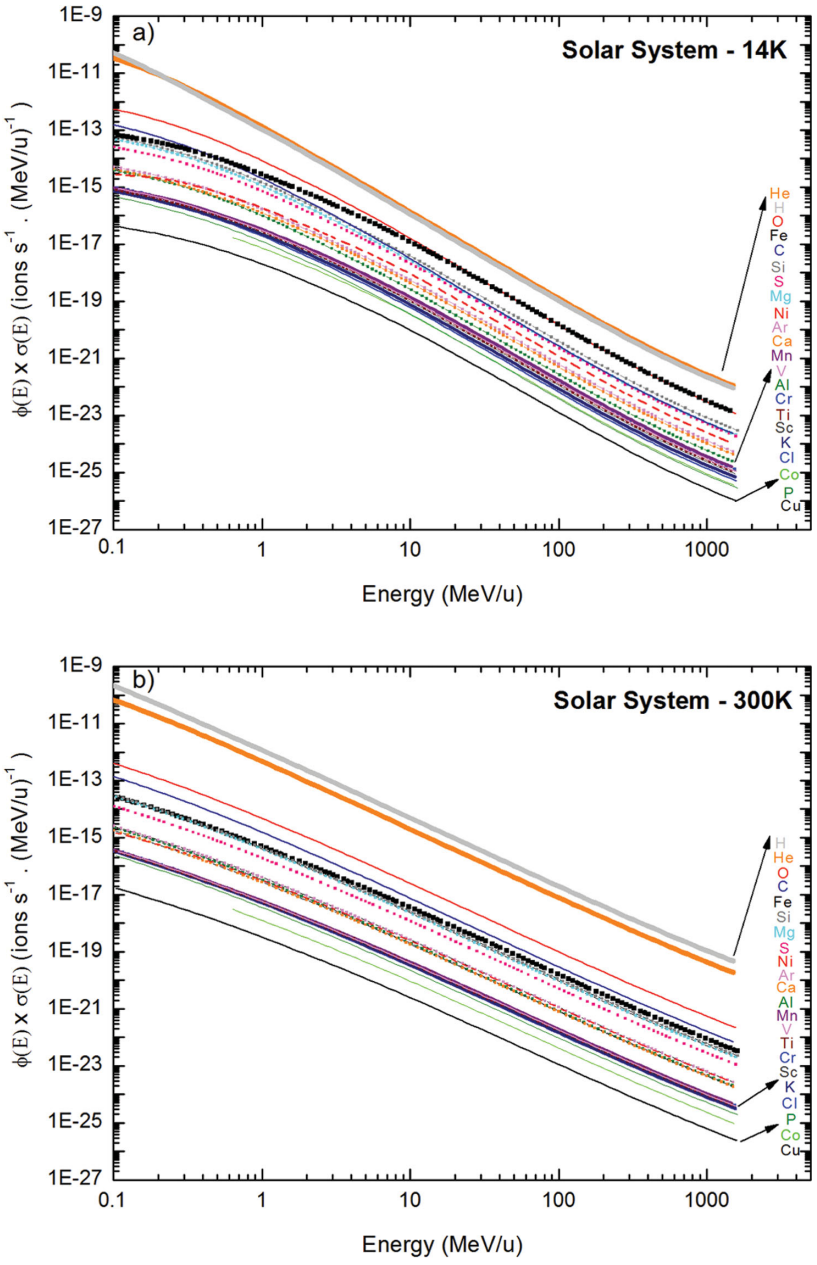

Figure 12. Differential dissociation rate of glycine by cosmic rays in the Solar system (SS) as a function of energy, for experiments at (a) 14 K and (b) 300 K.

exposed to heavy ions in the energy range ∼0.1–10 MeV, employing equation (13) of Pilling et al. (2010a,b):

$$\tau^* = \frac{\ln(2)}{\phi, \sigma_{\rm d}}, \tag{13}$$

where ϕ is the flux of heavy ion cm^{-2} s^{-1}, estimated by Pilling et al. (2010a,b), and $\sigma_{\rm d}$ is the dissociation cross-section in cm^2 determined in this work for 14 and 300 K. As discussed by Pilling et al. (2010a,b), an estimate for the flux of heavy ions ($12 \leq Z \leq 29$) with energy in range 0.1–10 MeV (a.m.u.)$^{-1}$ in the ISM is about 5×10^{-2} cm^{-2} s^{-1}. Inside the SS, at the Earth's orbit, the flux of such heavy ions (including the heavy component of cosmic rays plus energetic solar particles) in the same energy range is about 2×10^{-2} cm^{-2} s^{-1}. In this methodology, as a consequence of the higher dissociation cross-sections of the coldest sample, the half-life of glycine at 300 K was higher than that of glycine at 14 K. A variation of such stability with temperature was also verified by Gerakines et al. (2012). The results obtained in this work, involving the glycine cross-section for Ni ions with 46 MeV only, and the results obtained by Pilling et al. (2010a,b) suggest that the hottest regions in the ISM or SS could be a better target for glycine searches in space environments than the coldest regions. However, the half-lives estimated by Andrade et al. (2013) involve other variables, such as the flux and cross-section of each ion constituent of cosmic rays as a function of energy, showing that glycine survives for a longer time in the hottest environments of the ISM under the action of all ions. In the SS, the molecule can be better found in the coldest regions under the bombardment of all ions and in the hottest regions under the action of heavy ions only, without the action of H and He ions.

Table 7 lists values of half-life τ (in years) of the glycine molecule in the ISM and SS at 14 and 300 K exposed to cosmic ray irradiation.

Table 6. Ionization rates k (in s^{-1}) of the glycine molecule in the ISM and SS at 14 and 300 K exposed to cosmic rays, in energy ranges ∼0.1–1.5 MeV (a.m.u.)$^{-1}$ and ∼0.1–10 MeV (a.m.u.)$^{-1}$.

	ISM (dense clouds)		SS	
Ionization rate	14 K	300 K	14 K	300 K
k	7.92×10^{-12}	2.80×10^{-12}	6.15×10^{-12}	2.61×10^{-11}
k'	6.61×10^{-12}	1.86×10^{-12}	6.15×10^{-12}	2.61×10^{-11}
k_{HCR}	7.64×10^{-12}	1.69×10^{-12}	4.77×10^{-14}	1.43×10^{-14}
k'_{HCR}	6.46×10^{-12}	1.51×10^{-12}	4.77×10^{-14}	1.43×10^{-14}

k: ionization rate considering the most abundant ions ($12 \leq Z \leq 29$, H, He, C and O) with energy in range ∼0.1–1.5×10^3 MeV (a.m.u.)$^{-1}$.
k': ionization rate considering the most abundant ions ($12 \leq Z \leq 29$, H, He, C and O) with energy in range ∼0.1–10 MeV (a.m.u.)$^{-1}$.
k_{HCR}: ionization rate considering only heavy ions ($12 \leq Z \leq 29$) with energy in range ∼0.1–1.5×10^3 MeV (a.m.u.)$^{-1}$.
k'_{HCR}: ionization rate considering only heavy ions ($12 \leq Z \leq 29$) with energy in range ∼0.1–10 MeV (a.m.u.)$^{-1}$.

Table 7. Half-life τ (in years) of the glycine molecule in the ISM and SS, at 14 and 300 K exposed to cosmic ray irradiation. For comparison purposes, half-lives determined by Pilling et al. (2010a,b), named as τ^*, are also given. Finally, a correction factor (τ/τ^*) was calculated to correct the half-lives estimated using the Pilling et al. (2010a,b) methodology.

	ISM (dense clouds)		SS	
Half-life	14 K	300 K	14 K	300 K
τ	2.8×10^3	7.8×10^3	3.6×10^3	8.4×10^2
τ'	3.3×10^3	1.2×10^4	3.6×10^3	8.4×10^2
τ_{HCR}	2.9×10^3	1.3×10^4	4.6×10^5	1.5×10^6
τ'_{HCR}	3.4×10^3	1.4×10^4	4.6×10^5	1.5×10^6
τ / τ_{HCR}	∼1.0	0.6	7.8×10^{-3}	5.6×10^{-4}
τ^*	1.8×10^5	1.3×10^6	4.6×10^5	3.2×10^6
τ'_{HCR}/τ^*	0.02	0.01	1.0	0.5
τ/τ^*	0.02	0.006	0.008	0.00026

τ: half-life taking into account the most abundant ions ($12 \leq Z \leq 29$, H, He, C and O) with energy in range ∼0.1–1.5×10^3 MeV (a.m.u.)$^{-1}$.
τ': half-life considering the most abundant ions ($12 \leq Z \leq 29$, H, He, C and O) with energy in range ∼0.1–10 MeV (a.m.u.)$^{-1}$.
τ_{HCR}: half-life by interaction with heavy ions ($12 \leq Z \leq 29$) with energy in range ∼0.1–1.5×10^3 MeV (a.m.u.)$^{-1}$.
τ'_{HCR}: half-life by interaction with heavy ions ($12 \leq Z \leq 29$) with energy in range ∼0.1–10 MeV (a.m.u.)$^{-1}$.
τ^*: half-life determined employing previous methodology (Pilling et al. 2010a,b).

For comparison purposes, half-lives determined by Pilling et al. (2010a,b), named as τ^*, are also given. Finally, a correction factor (τ/τ^*) was calculated to correct the half-lives estimated using the Pilling et al. (2010a,b) methodology.

Table 8 shows a compilation of the half-life values for the α-glycine molecule in the ISM (dense clouds) under the action of a single ionizing agent obtained by different authors (Ferreira-Rodrigues et al. 2011; Pilling et al. 2011a; Gerakines et al. 2012). From this table, we can conclude that if we consider the glycine dissociation cross-section under the action of one ionizing agent only, the half-life increases. Exceptions occur for α-glycine under the bombardment of soft X-rays, due to the high dissociation cross-section molecules in this energy range (Pilling et al. 2011b).

Table 8. Half-life in years (τ) of the glycine molecule in the ISM (dense clouds) under the action of ionizing agents only, estimated by other authors, for comparison with the values obtained in this work.

Ionizing agent	Sample	τ (dense clouds)	Ref.
UV lamp (10 eV)	α-glycine negatively charged (300 K)	2.4×10^6	[1]
Soft X-rays (150 eV)	α-glycine (300 K)	1.8×10^2	[2]
Proton (0.8 MeV)	α-glycine (300 K)	7.6×10^6	[3]
$^{58}Ni^{11+}$ (46 MeV)	α-glycine (14 K)	$>3.0 \times 10^6$	[4]
	α-glycine (300 K)	$>1.5 \times 10^6$	[4]

(1) Ferreira-Rodrigues et al. (2011); (2) Pilling et al. (2011a); (3) Gerakines et al. (2012); (4) this work.

6 CONCLUSIONS

In this work we presented an experimental study of the stability of the amino acid glycine in the solid phase (crystalline α-glycine form) bombarded by 46-MeV $^{58}Ni^{11+}$ ions (∼0.8 MeV (a.m.u.)$^{-1}$). Samples at 14 and 300 K were exposed to a fluence of 1×10^{13} ion cm^{-2} at the GANIL heavy-ion accelerator, in an attempt to simulate the effects of heavy and energetic cosmic rays in astrophysical environments. The samples were analysed in situ by a Fourier transform infrared spectrometer. The dissociation cross-sections of glycine molecules were determined and half-lives for this species (hypothetically present) in different space regions and energy ranges were estimated. Our main results and conclusions are the following.

(i) Dissociation cross-section values were obtained for 14 K ($\sigma_d = 2.4 \times 10^{-12}$) and 300 K ($3.4 \times 10^{-13}$cm^2). The estimated error was about 20 and 50 per cent for the experiments at 14 and 300 K, respectively. Considering the average value between the different specific bond rupture cross-sections showed that at 14 K the glycine dissociation cross-section was about seven times higher than at room temperature. It was also possible to see that for any adopted vibration mode, or considering average values, the glycine dissociation cross-sections are higher for the sample at 14 K.

(ii) The formation and dissociation cross-sections of new species formed by bombardment of the sample at 14 K were also obtained. They are, respectively, CN^- (0.14×10^{-14} cm^2; $<0.1 \times 10^{-13}$ cm^2), CO (1.30×10^{-14} cm^2; $<0.1 \times 10^{-13}$ cm^2), OCN^- (0.24×10^{-14} cm^2; $<0.1 \times 10^{-13}$ cm^2), CO_2 (0.98×10^{-14} cm^2; $<0.1 \times 10^{-13}$ cm^2) and H_2O (4.20×10^{-14} cm^2; $<1.6 \times 10^{-13}$ cm^2). In the sample at 300 K, this species could have been formed but is not observed in the spectrum, suggesting it was desorbed. In the spectrum of glycine heated to 300 K, likewise this species is not observed.

(iii) The half-life of glycine extrapolated to the ISM was estimated to be 7.8×10^3 yr (for the 300 K sample) and 2.8×10^3 yr (14 K). In the Solar system (SS), the values were 8.4×10^2 yr (300 K) and 3.6×10^3 yr (14 K). This indicates that samples at higher temperature (in the ISM) have a higher half-life. The same relation was shown by Pilling et al. (2014) for glycine molecules in the presence of fast electrons. In the hottest environments of the SS, including the most abundant ion constituents of cosmic rays (heavy ions ($12 \leq Z \leq 29$), H, He, C and O ions), the glycine half-life is lower. This happens because the effect of heavy ions in the ISM is dominant for cosmic rays. Furthermore, the dissociation rate is higher at 14 K than at 300 K in the ISM. In the SS, the effects of light ions, specifically of H and He, which come mainly from the Sun, become more important. The effects of these ions are more intense inside the SS at the Earth's orbit and the glycine dissociation cross-sections for H and He ions are highest in the hottest environments of the SS. In view of these results, we can conclude

that glycine would survive during the formation of the SS under the constant bombardment of cosmic rays only if the molecule were protected, for example inside cometary surfaces or on interstellar grains. Furthermore, if the sample had thickness higher than the maximum ion penetration depth (e.g. $d > 17.5$ μm when considering only 46-MeV Ni ions), is possible that the deepest layers of an astrophysical ice with glycine would not be bombarded by ionizing particles. Therefore, the glycine would survive longer than the time estimation of the half-life of molecules in direct contact with the radiation field. According to Pilling et al. (2014), the question that remains is: does glycine form on grains in interstellar regions and persist to solar system formation, or is it a molecule formed and destroyed many times during the star and planet formation cycle? This work also suggests that, due to the low resistance of the glycine sample inside the radiation field of the SS, a considerable fraction could have been produced later in SS evolution and persisted to seed the origins of life.

(iv) Comparing two distinct methodologies concerning the contribution of different cosmic ray constituents in the destruction of glycine in space analogue environments (e.g Andrade et al. 2013; Pilling et al. 2010a,b), it is possible to correct the values of half-life by factors (τ/τ^*) (Table 7). These factors can be used in future investigations to correct the half-lives of glycine estimated using the Pilling et al. (2010a,b) methodology.

(v) The production of water in the sample during ion bombardment may be related to formation of the peptide bond. In addition, the possible identification of amide vibrational modes around 1650 and 1590 cm^{-1} in the infrared spectra of the bombarded samples reinforces this scenario of peptide bond formation. However, since several other chemical pathways may lead to the formation of water (including residual gas deposition in the substrate) and also to the formation of molecules containing amide groups, the peptide bond formation suggested here must be employed with caution. Future experiments, for example using isotopic labelling, may help to clarify this issue.

It is believed that α-glycine would be present in space environments that suffered aqueous changes, such as the interiors of comets, meteorites and planetesimals, as discussed by Pilling et al. (2013). Therefore, it could contribute to the start of prebiotic chemistry on our planet, if glycine molecules were protected against constant bombardment by cosmic rays, for example inside cometary surfaces or in interstellar grains. Thus, the study of the stability of glycine in these environments, under ion bombardment, provides further understanding of the role of this species in prebiotic chemistry on Earth.

ACKNOWLEDGEMENTS

The authors acknowledge the Brazilian agencies CAPES and CNPq for financial support. SP thanks T. Madi, A. Domaracka, C. Grygiel and I. Monnet, also the GANIL laboratory/CIMAP for partial financial support during the measurements and Th. Been and J. M. Ramillon for technical support. We also thank Ms Alene Alder Rangel for the English revision of this manuscript.

REFERENCES

Abdoul-Carime H., Sanche L., 2004, J. Phys. Chem. B, 108, 457
Anders C., Urbassek H. M., 2012, Nucl. Instr. Meth. B, 303, 200
Andrade D. P. P. et al., 2008, J. Phys. Chem. C, 112, 11954
Andrade D. P. P., de Barros A. L. F., Pilling S., Domaracka A., Rothard H., Boduch P., da Silveira E. F., 2013, MNRAS, 430, 787
Bergantini A., Pilling S., Rothard H., Boduch P., Andrade D. P. P., 2014, MNRAS, 437, 2720
Bernstein M. P., Dworkin J. P., Sandford S. A., Cooper G. W., Allamandola L. J., 2002, Nature, 416, 401
Blagojevic V., Petrie S., Bohme D. K., 2003, MNRAS, 339, L7
Boogert A. C. A., Ehrenfreund P., 2004, in Witt A. N., Clayton G. C., Draine B. T., eds, ASP Conf. Ser. 309, Interstellar Ices. Astron. Soc. Pac., San Francisco, p. 547
Bossa J.-B., Duvernay F., Theulé P., Borget F., d'Hendecourt L., Chiavassa T., 2009, A&A, 506, 601
Chyba C. F., Thomas P. J., Brookshaw L., Sagan C., 1990, Science, 249, 366
Chyba C., Sagan C., 1992, Nature, 355, 125
Collado V. M., Farenzena L. S., Ponciano C. R., da Silveira E. F., Wien K., 2004, Surf. Sci., 569, 149
Cronin J. R., Pizzarello S., 1983, Adv. Space Res., 3, 5
Cronin J. R., Pizzarello S., Cruikshank D. P., 1988, in Kerridge J. R., Matheus M. S., eds, Organic Matter in Carbonaceous Chondrites, Planetary Satellites, Asteroids and Comets. Univ. Arizona Press, Tucson, p. 819
de Barros A. L. F., Domaracka A., Andrade D. P. P., Boduch P., Rothard H., da Silveira E. F., 2011, MNRAS, 418, 1363
de Barros A. L. F., da Silveira E. F., Pilling S., Domaracka A., Rothard H., Boduch P., 2014, MNRAS, 438, 2026
de Marcellus P. et al., 2011, ApJ, 727, L27
Drury L. O. C., Meyer J.-P., Ellison D. C., 1999, in DuVernois M. A., ed., Topics in Cosmic-Ray Astrophysics. Nova Science Publishers, New-York
Ehrenfreund P., Charnley S. B., 2000, A&A, 38, 427
Ehrenfreund P., Bernstein M. P., Dworkin J. P., Sandford A., Allamandola L. J., 2001, ApJ, 550, L95
Elsila J. E., Dworkin J. P., Bernstein M. P., Martin M. P., Sandford S. A., 2007, ApJ, 660, 911
Elsila J. E., Glavin D. P., Dworkin J. P., 2009, Meteorit. Planet. Sci., 9, 1323
Ferreira-Rodrigues A. M., Homem M. G. P., Naves de Brito A., Ponciano C. R., da Silveira E. F., 2011, Int. J. Mass Spectrometry, 306, 77
Gerakines P. A., Scutte W. A., Greenberg J. M., van Dishoeck E. F., 1995, A&A, 296, 810
Gerakines P., Hudson R. L., Moore M. H., Bell J.-L., 2012, Icarus, 220, 647
Glavin D. P., Dworkin J. P., 2009, Proc. Natl Acad. Sci. USA, 106, 5487
Glavin D. P., Callahan M. P., Dworkin J. P., Elsila J. E., 2011, Meteorit. Planet. Sci., 45, 1948
Guan Y., Fray N., Coll P., Macari F., Chaput D., Raulin F., Cottin H., 2010. Planet. Space Sci., 58, 1327
Holtom P. D., Bennett C. J., Osamura Y., Mason N. J., Kaiser R. I., 2005, ApJ, 626, 940
Kaiser R. I., Stockton A. M., Kim Y. S., Jensen E. C., Mathies R. A., 2013, AJ, 765, 111
Kobayashi K., Kaneko T., Takano Y., Takahashi J.-i., 2008, in Kwok S., Sandforf S., eds, Proc. IAU Symp. 251, Organic Matter in Space. Cambridge Univ. Press, UK, p. 465
Kuan Y.-J., Charnley S. B., Huang H.-C., Tseng W.-L., Kisiel Z., 2003, AJ, 593, 848
Largo A., Redondo P., Barrientos C., 2003, Int. J. Quantum Chem., 98, 355
Largo L., Redondo P., Rayón V. M., Largo A., Barrientos C., 2010, A&A, 516, A79
Liu Z., Zhong L., Ying P., Feng Z., Li C., 2008, Biophys. Chem., 132, 18
Maeda S., Ohno K., 2004, Chem. Phys. Lett, 398, 240
Mendoza C., Ruette F., Martorell G., Rodríguez L. S., 2004, ApJ, 601, L59
Miller S. L., 1953, Science, 117, 528
Miller S. L., 1955, J. Am. Chem. Soc., 77, 2351
Muñoz C. et al., 2002, Nature, 416, 403
Nuevo M., Auger G., Blanot D., D'Hendecourt L., 2008, Orig. Life Evol. Biosph., 38, 37
Oró J., 1961, Nature, 190, 389
Peeters Z., Botta O., Charnley S. B., Ruiterkamp R., Ehrenfreund P., 2003, AJ, 593, L129

Pilling S., Andrade D. P. P., Neto A. C., Rittner R., de Brito A. N., 2009, J. Phys. Chem. A., 113, 11161
Pilling S., Duarte E. S., da Silveira E. F., Balanzat E., Rothard H., Domaracka A., Boduch P., 2010a, A&A, 509, A87
Pilling S., Duarte E. S., Domaracka A., Rothard H., Boduch P., da Silveira E. F., 2010b, A&A, 523, A77
Pilling S., Baptista L., Boechat-Roberty H. M., Andrade D. P. P., 2011a, Astrobiology, 11, 883
Pilling S., Duarte E. S., Domaracka A., Rothard H., Boduch P., da Silveira E. S., 2011b, Phys. Chem. Chem. Phys., 13, 15755
Pilling S. et al., 2011c, MNRAS, 411, 2214
Pilling S., Andrade D. P. P., da Silveira E. S., Rothard H., Domaracka A., Boduch P., 2012, MNRAS, 423, 2209
Pilling S., Mendes L., Bordalo V., Guaman C., Ponciano C., da Silveira E., 2013, Astrobiology, 13, 79
Pilling S., Nair B. G., Escobar A., Fraser H., Mason N., 2014, Eur. Phys. J. D, 68, 58
Ponnamperuma C., Woeller F. H., 1967, Curr. Mod. Biol., 1, 156
Reis E. F., Campos F. S., Lage A. P., Leite R. C., Heneine L. G., Vasconcelos W. L., Lobato Z. I. P., Mansur H. S., 2006, Materials Res., 9, 185
Rimola A., Ugliengo P., 2009, Phys. Chem. Chem. Phys., 11, 2497
Sanchez R. A., Ferris J. P., Orgel L. E., 1966, Science, 154, 784
Seperuelo E. D., Boduch P., Rothard H., Been T., Dartois E., Farenzena L. S., da Silveira E. F., 2009, A&A, 502, 599
Shen C. J., Greenberg J. M., Schutte W. A., van Dishoeck E. F., 2004, A&A, 415, 203
Sorrell W. H., 2001, ApJ, 555, L129
ten Kate I. L., Garry J. R. C., Peeters Z., Quinn R., Foing B., Ehrenfreund P., 2005, Meteorit. Planet. Sci., 40, 1185
Weber A. L., Pizzarello S., 2006, PNAS, 103, 12713
Webber W. R., Yushak S. M., 1983, ApJ, 275, 391
Woon D. E., 2002, AJ, 571, 177
Zhu H.-S., Ho J.-J., 2004, J. Phys. Chem. A, 108, 3798
Ziegler J. F., Biersack J. P., Ziegler M. D., 2008, Stopping and Range of Ions in Matter – srim. SRIM Co, Chester, Maryland, available at: www.srim.org

APPENDIX A: PARAMETERS EMPLOYED IN THE COSMIC RAY FLUX

Table A1 lists some parameters employed in the model for the estimation of galactic and solar system cosmic rays.

Table A1. Relative abundances in the ISM and SS, normalization constant (C_z) and A_2 of several constituents of galactic cosmic rays related to the abundance of H.

Z	Element	Relative abundance of 10^6 H atoms (ISM)	Relative abundance of 3×10^8 H atoms (SS)	C_z (MI)	A_2 (SS)
1	H	10^{6}	3.00×10^{8}	9.42×10^{4}	46
2	He	$10^{4.8}$	6.00×10^{7}	6.30×10^{4}	9.2
4	C	$10^{3.4}$	7.54×10^{4}	236.6	1.16×10^{-2}
6	O	$10^{3.5}$	1.90×10^{5}	297.9	2.91×10^{-2}
12	Mg	$10^{2.8}$	1.19×10^{4}	59.4	1.82×10^{-3}
13	Al	$10^{1.7}$	9.50×10^{2}	4.7	1.46×10^{-4}
14	Si	$10^{2.8}$	1.19×10^{4}	59.4	1.82×10^{-3}
15	P	$10^{0.7}$	9.50×10	0.4	1.45×10^{-5}
16	S	$10^{1.9}$	4.75×10^{3}	7.5	7.30×10^{-4}
17	Cl	$10^{1.0}$	1.19×10^{2}	0.9	1.82×10^{-5}
18	Ar	$10^{1.1}$	9.48×10^{2}	1.2	1.45×10^{-4}
19	K	$10^{1.0}$	1.19×10^{2}	0.9	1.82×10^{-5}
20	Ca	$10^{1.6}$	6.00×10^{2}	3.8	9.20×10^{-5}
21	Sc	$10^{1.0}$	1.19×10^{2}	0.9	1.82×10^{-5}
22	Ti	$10^{1.0}$	1.19×10^{2}	0.9	1.82×10^{-5}
23	V	$10^{1.0}$	1.19×10^{2}	0.9	1.82×10^{-5}
24	Cr	$10^{1.0}$	1.19×10^{2}	0.9	1.82×10^{-5}
25	Mn	$10^{1.0}$	1.19×10^{2}	0.9	1.82×10^{-5}
26	Fe	$10^{2.8}$	9.48×10^{3}	59.4	1.45×10^{-3}
27	Co	$10^{0.08}$	2.38×10^{1}	0.11	3.65×10^{-6}
28	Ni	$10^{1.5}$	5.98×10^{2}	3.0	9.16×10^{-5}
29	Cu	$10^{-0.33}$	5.98	0.044	9.17×10^{-7}

This paper has been typeset from a TEX/LATEX file prepared by the author.